J. Fluid Mech. (2001), *vol.* 439, *pp.* 165–198. Printed in the United Kingdom

Laminar mixed convection in two-dimensional far wakes above heated/cooled bodies: model and experiments

By PETER EHRHARD

Forschungszentrum Karlsruhe, Institut für Kern- und Energietechnik, Postfach 3640, D-76021 Karlsruhe, Germany

(Received 21 September 1999 and in revised form 7 June 2000)

A heated or cooled body is positioned in a vertically rising forced flow. This develops both a kinematic and a thermal wake, the latter adding buoyant effects to the otherwise forced flow field. An asymptotic model is developed to treat this mixed convection in both plane and axisymmetric geometry. The model holds for laminar flow in the boundary layer approximation and uses a far-wake expansion for weak buoyant forces. For plane geometry the model is validated against both experiments in water and FEM simulations.

It is found for a heated wake that buoyant forces accelerate the fluid in the thermal wake such that the vertical velocity deficit in the kinematic wake is reduced. For strong heating this may even lead to vertical velocities larger than the forced flow amplitude. In conjunction the entrainment is intensified in a heated wake. The effects in a cooled wake are opposite in that the vertical velocity deficit is increased within the thermal wake and the horizontal flow into the wake is weakened. In a strongly cooled wake the horizontal flow may even invert, going from the wake centre into the ambient. The Prandtl number controls the width of the thermal wake and, thus, the portion of the kinematic wake which is affected by buoyant forces. Large Prandtl numbers superimpose a narrow buoyant plume, small Prandtl numbers a wide buoyant plume, onto the kinematic wake.

1. Introduction

Problems involving the combined effects of forced and natural heat convection have received little attention. This seems to be the case because in most practical applications either the forced convection or the natural convection dominates and the secondary effects can be neglected in a first approximation. In many important applications, however, both convective modes play an equally important role and, thus, have to be considered simultaneously. This article relates to such a problem.

We consider specifically a vertically rising forced flow, which passes in cross-flow a cylindrical (or spherical) body and develops a wake downstream. The body is at high temperature, such that the transferred heat leads to buoyant forces in the wake. This situation is of relevance for a number of engineering applications, e.g. hot-wire anemometry or heat exchangers. The flow is assumed to be laminar, which is true only in a limited range of parameters. Therefore, the practical relevance may be limited, as in many applications wake flows become turbulent due to inflection-type velocity profiles. The method of treating this mixed-convection problem, however, should apply likewise to turbulent flows in conjunction with simple (analytical) turbulence models.

We may roughly understand this mixed-convection problem as a superposition of a wake flow and a buoyant plume. The first ingredient, thus, is the wake flow. We shall focus on far laminar wakes. The theoretical treatment of far wakes starts with the work of Tollmien (1931). Based on boundary-layer theory he develops a first-order approximation to the asymptotic form of a plane far wake behind a slender body, valid for large distances downstream. Goldstein (1933) proceeds to a second-order approximation to the asymptotic form and, moreover, attempts to derive a third-order approximation but rejects it owing to its singular behaviour. It is Stewartson (1957), finally, who explains the origin of the difficulty at the third stage of approximation and who resolves the problem by adding an appropriate term. A detailed review and discussion of the stages of approximation is given by Berger (1971). In summary, for the plane far wake an asymptotic solution is available, refined to a third-order expansion. This solution in all stages of approximation gives self-similar velocity profiles far downstream of the body. For the axisymmetric far wake equivalent methods have been applied e.g. by Berger (1968) and an analogous asymptotic solution has been obtained. Again, Berger (1971) reviews the progress and the solution of the axisymmetric problem in full detail.

The second ingredient of this mixed-convection problem is the buoyant plume. Once more, we concentrate on the laminar flow and temperature field above a line (point) heat source. Plumes generated by free convection are the subject of numerous investigations. Zeldovich (1937) is to our knowledge the first author to theoretically recognize the self-similar form of flow and temperature fields in buoyant plumes. Schuh (1948) in turn presents a complete analysis based on boundary-layer theory. He derives the coupled set of differential equations and boundary conditions for the problem. Yih (1952) infers closed-form solutions to this set of equations for the specific Prandtl numbers $Pr = \frac{2}{3}, \frac{7}{3}$. A more complete theoretical treatment of plane laminar plumes is conducted by Fujii (1963). He derives a closed-form solution for $Pr = 2$ and, moreover, uses numerical integration to solve the two-point boundary value problem for $Pr = 0.01, 0.7, 10$. In addition to a further exact solution for $Pr = \frac{5}{9}$ by Brand & Lahey (1967), Gebhart, Pera & Schorr (1970) give a systematic review of the theoretical approaches and provide further solutions in the complete range $0.01 \leqslant Pr \leqslant 100$, obtained by numerical integration. A recent numerical, fully nonlinear treatment of the plane laminar problem is conducted by Liñán & Kurdyumov (1998). Further, asymptotic methods are used to develop solutions for the limiting cases of small and large Prandtl numbers by e.g. Spalding & Cruddace (1961) or Kuiken & Rotem (1971). The above list of theoretical studies is nowhere near complete, but an extensive review can be found in the book of Gebhart *et al.* (1988). There are corresponding experimental investigations of the problem in literature. The work of Rouse, Yih & Humphreys (1952) e.g. relates to a plane plume, rising above a line of small gas flames. Further examples are the experiments of Brodowicz & Kierkus (1966) or Forstrom & Sparrow (1967), where precise flow and temperature fields are measured above heated wires in air. Again, a complete review of the experimental investigations can be found in Gebhart *et al.* (1988).

To summarize, the problem of a plane, laminar plume above a line heat source can be treated within the framework of boundary-layer theory and self-similar solutions are obtained. The theoretical and experimental treatment of axisymmetric, laminar plumes has been developed to an equivalent stage, as discussed theoretically e.g. by Schuh (1948), Yih (1951), Fujii (1963), Brand & Lahey (1967), Crane (1975), experimentally e.g. by Rouse *et al.* (1952) and reviewed by Gebhart *et al.* (1988).

The combined occurrence of both phenomena, namely forced and natural convec-

tion behind a heated cylindrical or spherical body, has also been studied in the past. In a first class of theoretical investigations the body is idealized as a line or point heat source, positioned in an otherwise undisturbed, parallel flow. Thus, the presence of the body of finite size is ignored kinematically and only buoyant forces due to the introduced heat are present. Based on boundary-layer theory Afzal (1981) develops two expansions, valid for weak/strong buoyant forces in the near-/far-field of a line heat source. The forced flow is upward or downward in the gravitational field, such that buoyant forces are favourable or adverse with respect to the forced flow. The corresponding axisymmetric problem of mixed convection behind a point heat source is theoretically treated by Riley & Drake (1983), Afzal (1983) and Afzal (1985). All authors invoke boundary-layer theory and infer solutions by means of asymptotic methods. Riley & Drake (1983) develop two solutions for weak/strong buoyant forces, uniformly valid downstream of the heat source in the entire region. Similarly, in the study of Afzal (1983) two expansions for weak/strong buoyant forces in conjunction with a spatial reversal are obtained. Finally, Afzal (1985) presents a new formulation, capturing both the weakly and strongly buoyant regime in a single set of equations. Wesseling (1975), in contrast to the above authors, avoids the boundary-layer approximation and uses instead the Oseen–Boussinesq equations as the basis for his analysis. He develops asymptotic solutions for weak buoyant forces, which enable the field variables in the near field of the (line) point heat source to be accessed.

The second class of theoretical investigations considers the finite size of the body to some extent. Here, the deflection of the flow around the body, the no-slip condition and some thermal condition on the body contour arise. Wood (1972) develops a three-zone model for the plane mixed convection around a heated cylinder. He considers (i) an inner, diffusive zone immediately around the cylinder, (ii) a wake zone downstream of the cylinder and (iii) an outer zone with irrotational flow, and works out the dominant physics and coupling of these zones. The corresponding axisymmetric problem, i.e. mixed convection from a sphere, is treated by Hieber & Gebhart (1969).

There are corresponding experimental investigations of mixed convection from cylinders (wires) in the literature. Collis & Williams (1959) or Hatton, James & Swire (1970) are two examples. A more complete review of the experimental work can be found in Gebhart & Pera (1970). In summary, experiments cover a range of Prandtl numbers $0.7 \leqslant Pr \leqslant 63$ (air, silicone oils) and focus mostly on the integral heat transfer from the cylinder. Measurements of field variables around the body and downstream in the wake are not available to our knowledge.

The present article concentrates on the wake some distance downstream of a heated cylindrical (spherical) body. This follows to some extent the idea of Wood (1972), particularly with respect to the 'wake zone'. Based on boundary-layer theory, we shall develop an asymptotic model by means of a two-parameter expansion. The small parameters are (i) an inverse power of the downstream coordinate and (ii) the ratio of buoyancy and inertia forces. Thus, the model holds far downstream for weakly buoyant conditions. For such a model the details of the flow and temperature fields around the body are not relevant. Instead, an integral representation of the effects of the body is sufficient. First, the loss of momentum in the flow is introduced via the drag coefficient of the body. With respect to the pure wake, the model is of second order, in accordance with the expansions of Goldstein (1933) and Berger (1968). Secondly, an integral amount of heat is introduced at the position of the body. Here the present model is in accord with Wood (1972) as far as the plane formulation is concerned, but different in the presence of second-order, nonlinear terms, which allow

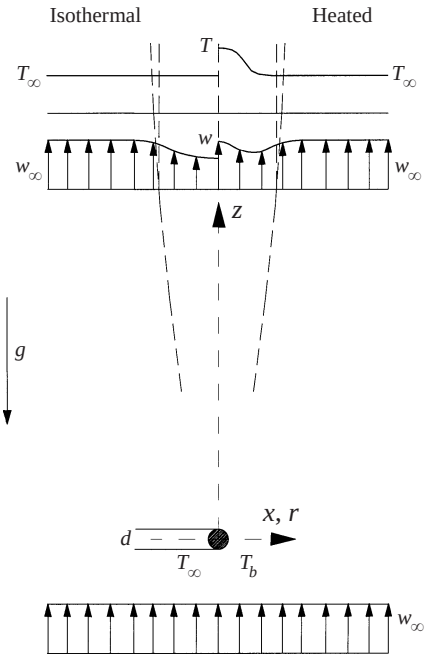

FIGURE 1. Sketch of the problem given for both an isothermal body and a heated body.

a more accurate description of the wake. The present axisymmetric formulation is given for the first time in literature.

The results from the asymptotic models are for both flow and temperature fields elaborated for realistic values of the parameters. This goes beyond the intention of Wood (1972). Detailed experiments in water, capturing all field variables downstream of a cylinder are also carried out to verify the results from the asymptotic model. Such experiments are to our knowledge not yet available in the literature. Numerical (FEM) simulations of the full plane problem serve as a further means to elucidate possible deficiencies of the approximations.

2. Formulation

2.1. *Description of the problem*

Let us consider a cylindrical or spherical body in a parallel flow of speed w_∞ and temperature T_∞ as sketched in figure 1. The flow is upward against the gravitational field. In addition, through a constant body temperature $T_b \geqslant T_\infty$, an integral heat flux $\dot{Q}$ (respectively a heat flux per unit length $\dot{q}$ for the plane problem) can be added to the flow. First, for $T_b = T_\infty$, due to the presence of the body alone the flow will be deflected as it passes the body. For sufficiently small w_∞ we shall have a steady and laminar flow. The second effect of the body is due to the no-slip condition on the body contour, resulting in an integral loss of momentum. Consequently a drag force F_z (respectively a drag force per unit length f_z for the plane problem) applies to the body and reduced velocity amplitudes are present in the wake. Up to this point we have no buoyant effects involved. If we heat the body to $T_b > T_\infty$, thirdly, we will have hot fluid in the wake. Thus, buoyant forces will tend to accelerate the fluid in the wake.

2.2. *Basic equations and scaling*

If we consider a Newtonian fluid and invoke the Boussinesq approximation, the steady velocity and temperature fields in the fluid are governed by the Navier–Stokes, the continuity and the heat transport equations. Thus, we have

$$\rho_\infty(\boldsymbol{v}\cdot\nabla)v = -\nabla p + \mu\nabla^2 v + \alpha g\rho_\infty(T - T_\infty)\boldsymbol{e}_z, \tag{2.1}$$

$$\nabla\cdot\boldsymbol{v} = 0, \tag{2.2}$$

$$\rho_\infty c_p(\boldsymbol{v}\cdot\nabla)T = \lambda\nabla^2 T. \tag{2.3}$$

Here $e_z = (0,0,1)$ is the unit vector in the z-direction and the velocity vector is given by $v = (u,v,w)$. The deviation from a hydrostatic pressure field is denoted by p and T is the temperature of the fluid. The material properties of the fluid $\rho_\infty, \mu, c_p, \lambda$ denote density, viscosity, specific heat and heat conductivity, which are all taken to be constant. The buoyant term has a linear dependence on temperature T around the reference density ρ_∞ (at T_∞). Volume expansion α and gravitational acceleration g are likewise constant.

The above conservation equations for momentum, mass and energy in the two-dimensional problem are subject to the boundary conditions (where p in the equation number refers to a plane geometry and a to an axisymmetric geometry)

$$x, z \to \pm\infty: \quad u \to 0, \quad w \to w_\infty, \quad T \to T_\infty, \tag{2.4p}$$

$$x = 0, |z| > \tfrac{1}{2}d: \quad u = 0, \quad \frac{\partial w}{\partial x} = 0, \quad \frac{\partial T}{\partial x} = 0, \tag{2.5p}$$

$$x \to \pm\infty, z: \quad \frac{\partial u}{\partial x} \to 0, \quad w \to w_\infty, \quad T \to T_\infty, \tag{2.6p}$$

$$\sqrt{x^2+z^2} = \tfrac{1}{2}d: \quad u = 0, \quad w = 0, \quad T = T_b; \tag{2.7p}$$

$$r, z \to \pm\infty: \quad u \to 0, \quad w \to w_\infty, \quad T \to T_\infty, \tag{2.4a}$$

$$r = 0, |z| > \tfrac{1}{2}d: \quad u = 0, \quad \frac{\partial w}{\partial r} = 0, \quad \frac{\partial T}{\partial r} = 0, \tag{2.5a}$$

$$r \to \infty, z: \quad \frac{\partial u}{\partial r} \to 0, \quad w \to w_\infty, \quad T \to T_\infty, \tag{2.6a}$$

$$\sqrt{r^2+z^2} = \tfrac{1}{2}d: \quad u = 0, \quad w = 0, \quad T = T_b. \tag{2.7a}$$

Thus, we assume an undisturbed parallel and isothermal flow both far upstream and far downstream of the body. Symmetry with respect to both velocity and temperature fields is assumed with respect to the z-axis. On the body contour (cylinder, sphere) the no-slip condition and a constant temperature is applied. Sufficiently far from the body the flow is undisturbed with respect to w_∞ and T_∞, allowing in general a non-zero u in that region.

It is convenient at this stage to scale the problem in order to infer both dimensionless equations and dimensionless groups. We use the scales

$$(X,Z) = \frac{(x,z)}{d}, \quad (R,Z) = \frac{(r,z)}{d}, \tag{2.8p,a}$$

$$(U, W) = \frac{(u, w)}{w_\infty}, \tag{2.9}$$

$$P = \frac{p}{\rho_\infty w_\infty^2}, \tag{2.10}$$

$$\Theta = \frac{(T - T_\infty)}{(T_b - T_\infty)}, \tag{2.11}$$

and, therefrom, obtain the dimensionless set of conservation equations

$$(\boldsymbol{V} \cdot \nabla)\boldsymbol{V} = -\nabla P + \frac{1}{Re}\nabla^2 \boldsymbol{V} + \frac{Gr}{Re^2}\Theta\, \boldsymbol{e}_Z, \tag{2.12}$$

$$\nabla \cdot \boldsymbol{V} = 0, \tag{2.13}$$

$$(\boldsymbol{V} \cdot \nabla)\Theta = \frac{1}{PrRe}\nabla^2 \Theta, \tag{2.14}$$

and boundary conditions

$$X, Z \to \pm\infty: \quad U \to 0, \quad W \to 1, \quad \Theta \to 0, \tag{2.15p}$$

$$X = 0, |Z| > \tfrac{1}{2}: \quad U = 0, \quad \frac{\partial W}{\partial X} = 0, \quad \frac{\partial \Theta}{\partial X} = 0, \tag{2.16p}$$

$$X \to \pm\infty, Z: \quad \frac{\partial U}{\partial X} \to 0, \quad W \to 1, \quad \Theta \to 0, \tag{2.17p}$$

$$\sqrt{X^2 + Z^2} = \tfrac{1}{2}: \quad U = 0, \quad W = 0, \quad \Theta = 1. \tag{2.18p}$$

$$R, Z \to \pm\infty: \quad U \to 0, \quad W \to 1, \quad \Theta \to 0, \tag{2.15a}$$

$$R = 0, |Z| > \tfrac{1}{2}: \quad U = 0, \quad \frac{\partial W}{\partial R} = 0, \quad \frac{\partial \Theta}{\partial R} = 0, \tag{2.16a}$$

$$R \to \infty, Z: \quad \frac{\partial U}{\partial R} \to 0, \quad W \to 1, \quad \Theta \to 0, \tag{2.17a}$$

$$\sqrt{R^2 + Z^2} = \tfrac{1}{2}: \quad U = 0, \quad W = 0, \quad \Theta = 1. \tag{2.18a}$$

The above scaling assumes the forced flow around the body to be dominant and, thus, uses the diameter d of the body, the far-field velocity w_∞ and the dynamic pressure ($\rho_\infty w_\infty^2$) to normalize length, velocity and pressure. The temperature scale is constructed using the applied temperature difference ($T_b - T_\infty$) such that $0 \leqslant \Theta \leqslant 1$ holds. The dimensionless groups in the above conservation equations (2.12)–(2.14) are identified as Reynolds number, Grashof number and Prandtl number. The definitions are

$$Re = \frac{w_\infty d}{\nu}, \tag{2.19}$$

$$Gr = \frac{\alpha g (T_b - T_\infty) d^3}{\nu^2}, \tag{2.20}$$

$$Pr = \frac{\nu}{\kappa}. \tag{2.21}$$

The Reynolds number characterizes the strength of the forced flow, the Grashof number provides a measure of the strength of the buoyant effects and the Prandtl number is a fluid property, characterizing the fluid with respect to the molecular diffusion of momentum and heat.

We can now characterize the plane flow around a cylinder for forced-flow conditions based on the Reynold number. According to e.g. Žukauskas & Žiugžda (1985) we find for $Re < 1$ a steady flow around the cylinder without separation. In the range $3 < Re < 5$ a separation immediately behind the cylinder with two symmetric vortices develops. For $Re < 40$ the flow remains steady and the size of the separation zone downstream increases. For $Re > 40$ the flow develops time-dependence in form of the so-called von-Kármán vortex street, featuring periodic vortex detachment. We can, therefore, conclude that for forced flow conditions we shall observe a steady plane wake behind the cylinder in the range $Re < 40$ and shall keep to this range in this article.

The axisymmetric flow behind a sphere behaves similarly. Following e.g. Lugt (1979) the flow remains attached for $Re < 20$. In the range $20 < Re < 400$ a torus-shaped steady recirculating vortex behind the sphere is present. For $Re > 400$ unsteady behaviour develops. If we therefore restrict the analysis to $Re < 400$ we shall observe a steady axisymmetric wake behind the sphere. In general, bodies of more streamlined shape exhibit a wider range of Reynolds numbers in which a steady wake, plane or axisymmetric, is observed. This is important to note, as the asymptotic model applies in the far wake for bodies of arbitrary shape.

In principle, there are two possible reasons for a time-dependent wake. The first is the flow described above in the near field around the body. The second might be an instability of the velocity profile in the wake further downstream. Following Betchov & Criminale (1967) inflection-type velocity profiles, as present in a heated wake, tend to become unstable for $Re_{ip} > 200$. The Reynolds number Re_{ip} is defined based on the shear layer thickness $(\delta/2)$ and the velocity difference $[w_\infty - w(0,z)]$ in the wake, i.e.

$$Re_{ip} = \frac{[w_\infty - w(0,z)]\delta}{2\nu}. \tag{2.22}$$

As we focus on steady wakes here, we always have to ensure that both conditions ensure both a steady near-field flow around the body and a stable (and thus steady) velocity profile in the wake further downstream. However, it remains uncertain to what extent the buoyant acceleration of the fluid affects the stability of the inflection-type velocity profile in the wake. Similarly, the buoyant forces may influence the flow in the near field of the heated body and, hence, influence the steady/time-dependent transition. As we shall concentrate on weakly heated bodies throughout most of this article, we consider these effects to be of minor importance.

2.3. *FEM simulation of the plane flow*

In order to obtain a full solution to the plane problem, we solve the above dimensionless equations (2.12)–(2.14) numerically, using the standard finite-element (FEM) code FIDAP 7.6. Although the boundary conditions (2.15)–(2.18) are mathematically formulated partly at infinite distances from the cylinder, we have to restrict the computational domain to a reasonable size, while the appropriate boundary conditions have to be formulated on the boundaries of the computational domain. Numerous tests have led us to chose the range of spatial coordinates for the numerical simulation as

$$0 \leqslant X \leqslant 30, \tag{2.23p}$$

$$-50 \leqslant Z \leqslant 60. \tag{2.24p}$$

Thus, for reasons of symmetry, we discretize one half of the flow field, and grid that region using nine-node quadrilateral elements, which employ biquadratic interpolation functions to approximate the velocity and temperature degrees of freedom within

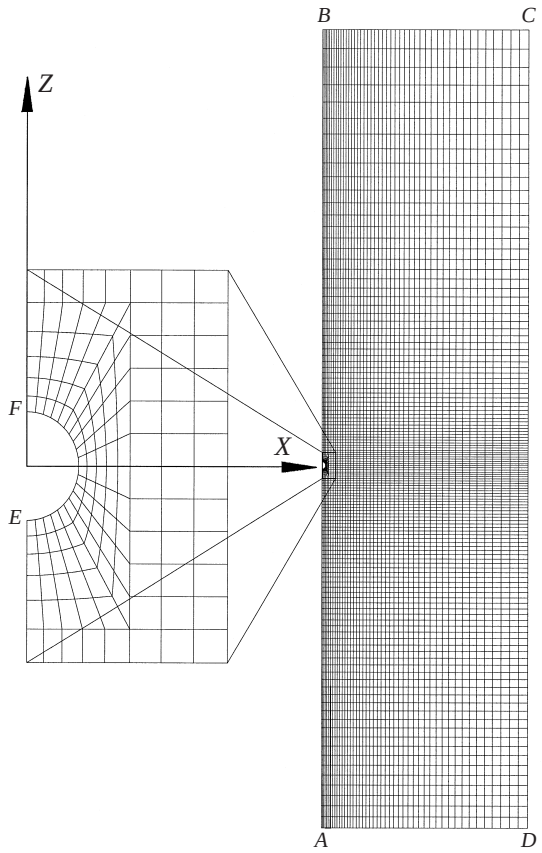

FIGURE 2. The FEM standard mesh employed.

each element. The standard mesh for the computations is shown in figure 2. From the details of the mesh around the cylinder, shown enlarged in figure 2, it is clear that we employ mostly rectangular elements and only depart from rectangles in the immediate vicinity of the cylinder. Here, a transition region is constructed to integrate the cylinder geometry into the rectangular computational domain. The aspect ratio of the elements has been kept close to one in all high-gradient regions. Very few elements, in particular in the outlet plane $\overline{CB}$, have aspect ratios which depart from one and it is at most 1 : 12. For standard computations we use about 6000 elements, corresponding to about 25 000 nodes, whereas numerous tests with strongly refined meshes and strongly increased computational domain have proven that all velocity and temperature profiles in the wake ($5 \leqslant Z \leqslant 50$) experience very little relative change. Thus, we are confident that our standard mesh in extent and refinement guarantees a solution which is accurate to $\pm 0.2\%$. Typical computations on an IBM RS/6000-580 workstation with 256 MB RAM take around 2000 CPU seconds.

In addition, we have installed a procedure that allows integration of all variables of the solution (and functions therefrom) along boundaries of the computational domain and around the cylinder contour. This integration is based on a trapezoidal scheme and allows e.g. the integral mass balance to be checked; it always remains accurate to $\pm 0.1\%$. Moreover, this procedure allows, from the velocity and temperature on those boundaries, the integral amount of heat $\dot{q}$ (per unit length), which has been transferred

into the flow to be inferred. In a similar fashion an integral balance of the momentum flux is computed, which leads to a determination of the force (per unit length) f_z acting on the cylinder for the case of pure forced flow. Depending on whether buoyant forces are present, the control volume is either the entire computational domain (forced flow) or the cylinder contour (mixed convection). The determination of $\dot{q}$ and f_z is essential as input for the asymptotic model (cf. § 2.4).

The boundary conditions which we apply to the computational domain have to depart from the ideal ones formulated in equations (2.15)–(2.18) for several reasons. We use

$$0 \leqslant X \leqslant 30, Z = -50, (\overline{AD}): \quad U = 0, \quad W = 1, \quad \Theta = 0, \tag{2.25p}$$

$$0 \leqslant X \leqslant 30, Z = 60, (\overline{BC}): \quad \frac{\partial U}{\partial Z} = 0, \quad \frac{\partial W}{\partial Z} - \frac{Re}{2} P = 0, \quad \frac{\partial \Theta}{\partial Z} = 0, \tag{2.26p}$$

$$X = 0, -50 \leqslant Z \leqslant -\tfrac{1}{2}, (\overline{AE}): \quad U = 0, \quad \frac{\partial W}{\partial X} = 0, \quad \frac{\partial \Theta}{\partial X} = 0, \tag{2.27p}$$

$$X = 0, \tfrac{1}{2} \leqslant Z \leqslant 60, (\overline{FB}): \quad U = 0, \quad \frac{\partial W}{\partial X} = 0, \quad \frac{\partial \Theta}{\partial X} = 0, \tag{2.28p}$$

$$X = 30, -50 \leqslant Z \leqslant 60, (\overline{CD}): \quad \frac{\partial U}{\partial X} = 0, \quad \frac{\partial W}{\partial X} = 0, \quad \Theta = 0, \tag{2.29p}$$

$$\sqrt{X^2 + Z^2} = \tfrac{1}{2}, (\overline{EF}): \quad U = 0, \quad W = 0, \quad \Theta = 1. \tag{2.30p}$$

Thus, mainly on the outflow boundary $\overline{BC}$ and on the side boundary $\overline{CD}$ the conditions are modified such that the decaying profiles of velocities and temperature are disturbed as little as possible. The set given here proves to behave in that manner.

2.4. *Asymptotic model for the far wake of weakly heated bodies*

It is well known in the literature (cf. Schlichting 1982) that far laminar (and even turbulent) wakes behind bodies, both plane and axisymmetric, are described well using the boundary-layer approximation. Similarly, buoyant plumes, at a sufficiently large distance above both line and point heat sources, allow theoretical modelling based on boundary-layer theory. As both single effects in the problem develop a boundary-layer type of flow sufficiently far downstream, it seems reasonable to expect that the combined and aligned occurrence in a buoyant wake above a heated body likewise results in a flow field which has a boundary-layer character.

Secondly the model assumes a dominant forced flow wake, only weakly disturbed by buoyant forces. This assumption allows the flow and temperature fields to be expressed in a much simpler fashion compared to the full problem given in equations (2.12)–(2.18). It should be pointed out that the following asymptotic model holds for bodies of arbitrary shape of plane or axisymmetric geometry. This is a consequence of the far-wake expansion, where the near field around the body is not resolved.

Both the far wake and the buoyant plume, whether plane or axisymmetric, within a boundary-layer approximation will lead to a power-law dependence on the streamwise coordinate Z. As discussed e.g. by Berger (1971) for the far wake, the (singular) origin $Z = 0$ of the power law is not identical to the centre of the body, nor to the trailing edge. A similar statement should hold for the buoyant plume with respect to the (singular) heat source. Taking the origin $Z = 0$ in the centre of the heated body is thus an approximation in several respects, while the error due to this approximation decays rapidly with increasing distance Z.

2.4.1. *Rescaling and boundary-layer approximation*

If we focus on the boundary-layer type of flow sufficiently far downstream above the body, it is reasonable to rescale the spatial coordinates such that the separate scales within the boundary layer are reflected. The scaling (2.8)–(2.11), therefore, is modified with respect to the horizontal coordinates and velocity. We apply

$$\tilde{X} = \frac{x}{(d/\sqrt{Re})} = \sqrt{Re}X, \quad \tilde{R} = \frac{r}{(d/\sqrt{Re})} = \sqrt{Re}R, \tag{2.31p, a}$$

$$\tilde{U} = \frac{u}{(w_\infty/\sqrt{Re})} = \sqrt{Re}U. \tag{2.32}$$

This separates the spatial scales by introducing the small parameter $\epsilon_1 = (1/\sqrt{Re})$. Further, we take advantage of the smallness of ϵ_1, i.e. we restrict ourselves to the case

$$\sqrt{Re} \gg 1, \tag{2.33}$$

and readily infer the leading order of an asymptotic expansion of the conservation equations (2.12)–(2.14). Thus, we obtain the boundary-layer equations for the problem, namely

$$\tilde{U}\frac{\partial W}{\partial \tilde{X}} + W\frac{\partial W}{\partial Z} = \frac{\partial^2 W}{\partial \tilde{X}^2} + \frac{Gr}{Re^2}\Theta + O\left(\frac{1}{Re}\right), \tag{2.34p}$$

$$\frac{\partial \tilde{U}}{\partial \tilde{X}} + \frac{\partial W}{\partial Z} = 0, \tag{2.35p}$$

$$\tilde{U}\frac{\partial \Theta}{\partial \tilde{X}} + W\frac{\partial \Theta}{\partial Z} = \frac{1}{Pr}\frac{\partial^2 \Theta}{\partial \tilde{X}^2} + O\left(\frac{1}{PrRe}\right); \tag{2.36p}$$

$$\tilde{U}\frac{\partial W}{\partial \tilde{R}} + W\frac{\partial W}{\partial Z} = \frac{\partial^2 W}{\partial \tilde{R}^2} + \frac{1}{\tilde{R}}\frac{\partial W}{\partial \tilde{R}} + \frac{Gr}{Re^2}\Theta + O\left(\frac{1}{Re}\right), \tag{2.34a}$$

$$\frac{\partial(\tilde{R}\tilde{U})}{\partial \tilde{R}} + \frac{\partial(\tilde{R}W)}{\partial Z} = 0, \tag{2.35a}$$

$$\tilde{U}\frac{\partial \Theta}{\partial \tilde{R}} + W\frac{\partial \Theta}{\partial Z} = \frac{1}{Pr}\left(\frac{\partial^2 \Theta}{\partial \tilde{R}^2} + \frac{1}{\tilde{R}}\frac{\partial \Theta}{\partial \tilde{R}}\right) + O\left(\frac{1}{PrRe}\right). \tag{2.36a}$$

As is clear from the accuracy of approximation within the heat transport equation (2.36) given above, we restrict ourselves additionally to fluids with Prandtl numbers that are not too small, i.e. we assume

$$\sqrt{PrRe} \gg 1. \tag{2.37}$$

The boundary conditions within this approximation reduce to

$$\tilde{X} = 0, Z > 0: \quad U = 0, \quad \frac{\partial W}{\partial \tilde{X}} = 0, \quad \frac{\partial \Theta}{\partial \tilde{X}} = 0, \tag{2.38p}$$

$$\tilde{X} \to \pm\infty, Z > 0: \quad W \to 1, \quad \Theta \to 0; \tag{2.39p}$$

$$\tilde{R} = 0, Z > 0: \quad U = 0, \quad \frac{\partial W}{\partial \tilde{R}} = 0, \quad \frac{\partial \Theta}{\partial \tilde{R}} = 0, \tag{2.38a}$$

$$\tilde{R} \to \infty, Z > 0: \quad W \to 1, \quad \Theta \to 0. \tag{2.39a}$$

Since the asymptotic model is valid only far downstream of the body, the no-slip and isothermal condition on the body contour cannot be enforced. Instead, we have to specify integral conditions for both the flux of momentum and the flux of heat. We chose a sufficiently large control volume around the body and balance mass, momentum and heat across the boundaries of the control volume. The drag force (respectively the drag force per unit length in the plane problem) is linked via

$$f_z = c_w \frac{\rho_\infty w_\infty^2}{2} d, \quad F_z = c_w \frac{\rho_\infty w_\infty^2}{2} \frac{\pi d^2}{4}, \tag{2.40p,a}$$

to the dimensionless drag coefficient c_w, the dynamic pressure and the cross-sectional area (respectively cross-sectional area per unit length for the plane problem) of the body. At the centre of the body we allow additionally for the input of an integral heat flux $\dot{Q}$ (respectively an integral heat flux per unit length $\dot{q}$ for the plane problem) into the flow. Within the framework of the boundary-layer approximation the integral conditions for the flux of momentum and the flux of heat turn out to be

$$\tfrac{1}{2} c_w = \frac{f_z}{\rho_\infty w_\infty^2 d} = \frac{1}{\sqrt{Re}} \left[\int_{-\infty}^{\infty} W(1-W)\,\mathrm{d}\tilde{X} + \frac{Gr}{Re^2} \int_{-\infty}^{Z} \int_{-\infty}^{\infty} \Theta\,\mathrm{d}\tilde{X}\,\mathrm{d}Z + O\left(\frac{1}{Re}\right) \right], \tag{2.41p}$$

$$\Omega = \frac{\dot{q}}{\rho_\infty c_p (T_b - T_\infty) v} = \sqrt{Re} \left[\int_{-\infty}^{\infty} W \Theta \mathrm{d}\tilde{X} + O\left(\frac{1}{PrRe}\right) \right]; \tag{2.42p}$$

$$\tfrac{1}{16} c_w = \frac{F_z}{\rho_\infty w_\infty^2 2\pi d^2}$$

$$= \frac{1}{Re} \left[\int_0^{\infty} \tilde{R} W(1-W)\,\mathrm{d}\tilde{R} + \frac{Gr}{Re^2} \int_{-\infty}^{Z} \int_0^{\infty} \tilde{R}\Theta \mathrm{d}\tilde{R}\,\mathrm{d}Z + O\left(\frac{1}{Re}\right) \right], \tag{2.41a}$$

$$\Omega = \frac{\dot{Q}}{\rho_\infty c_p d (T_b - T_\infty) v} = 2\pi \int_0^{\infty} \tilde{R} W \Theta \mathrm{d}\tilde{R} + O\left(\frac{1}{PrRe}\right). \tag{2.42a}$$

The dimensionless group Ω quantifies the integral amount of heat transferred to the body. It is linked to the a Nusselt number, as shown in § 3.2.

2.4.2. *Asymptotic expansion for the far wake*

As we consider the development of the wake as the dominant physics in the problem, it is appropriate to invoke the approximations for the description of far wakes, as e.g. given by Schlichting (1982). This is, as we shall see, another asymptotic expansion in terms of the small parameter

$$\epsilon_2 = 1/\sqrt{Z}, \quad \epsilon_2 = 1/Z. \tag{2.43p,a}$$

Formally, we apply the expansions

$$\tilde{U} = \epsilon_2 U_1 + \epsilon_2^2 U_2 + \cdots, \tag{2.44}$$

$$W = 1 - \epsilon_2 W_1 - \epsilon_2^2 W_2 + \cdots, \tag{2.45}$$

$$\Theta = \epsilon_2 \Theta_1 + \epsilon_2^2 \Theta_2 + \cdots, \tag{2.46}$$

which are strictly valid in the limit $\epsilon_2 \to 0$. At this stage we have to decide on the

magnitude of the buoyant term in the momentum equations (2.34). As mentioned above, we shall consider only weak buoyant effects. Thus, we chose the Grashof number such that

$$\frac{Gr}{Re^2} = O(\epsilon_2) \tag{2.47}$$

holds. This restricts the validity of the model with respect to large Gr. On the other hand it allows the buoyant term to be shifted into the second order of the expansion and, thus, provides a means of developing a solution. We shall discuss the range of validity of the model below in full detail. Using the expansions (2.44)–(2.46) and the magnitude of Gr in (2.47), we are able to break up the problem into an infinite number of simpler problems, and the two leading orders will be solved subsequently. The equations of the first order are homogeneous and are found to be

$$\frac{1}{\epsilon_2}\frac{\partial(\epsilon_2 W_1)}{\partial Z} - \frac{\partial^2 W_1}{\partial \tilde{X}^2} = 0, \tag{2.48p}$$

$$\frac{\partial U_1}{\partial \tilde{X}} - \frac{1}{\epsilon_2}\frac{\partial(\epsilon_2 W_1)}{\partial Z} = 0, \tag{2.49p}$$

$$\frac{1}{\epsilon_2}\frac{\partial(\epsilon_2 \Theta_1)}{\partial Z} - \frac{1}{Pr}\frac{\partial^2 \Theta_1}{\partial \tilde{X}^2} = 0; \tag{2.50p}$$

$$\frac{1}{\epsilon_2}\frac{\partial(\epsilon_2 W_1)}{\partial Z} - \left(\frac{\partial^2 W_1}{\partial \tilde{R}^2} + \frac{1}{\tilde{R}}\frac{\partial W_1}{\partial \tilde{R}}\right) = 0, \tag{2.48a}$$

$$\frac{\partial(\tilde{R} U_1)}{\partial \tilde{R}} - \frac{\tilde{R}}{\epsilon_2}\frac{\partial(\epsilon_2 W_1)}{\partial Z} = 0, \tag{2.49a}$$

$$\frac{1}{\epsilon_2}\frac{\partial(\epsilon_2 \Theta_1)}{\partial Z} - \frac{1}{Pr}\left(\frac{\partial^2 \Theta_1}{\partial \tilde{R}^2} + \frac{1}{\tilde{R}}\frac{\partial \Theta_1}{\partial \tilde{R}}\right) = 0, \tag{2.50a}$$

with the corresponding boundary and integral conditions

$$\tilde{X} = 0, Z > 0: \quad U_1 = 0, \quad \frac{\partial W_1}{\partial \tilde{X}} = 0, \quad \frac{\partial \Theta_1}{\partial \tilde{X}} = 0, \tag{2.51p}$$

$$\tilde{X} \to \pm\infty, Z > 0: \quad W_1 \to 0, \quad \Theta_1 \to 0, \tag{2.52p}$$

$$\int_{-\infty}^{\infty} W_1 \mathrm{d}\tilde{X} = \frac{c_w}{2}\sqrt{Re}\sqrt{Z}, \tag{2.53p}$$

$$\int_{-\infty}^{\infty} \Theta_1 \mathrm{d}\tilde{X} = \frac{\Omega\sqrt{Z}}{\sqrt{Re}}; \tag{2.54p}$$

$$\tilde{R} = 0, Z > 0: \quad U_1 = 0, \quad \frac{\partial W_1}{\partial \tilde{R}} = 0, \quad \frac{\partial \Theta_1}{\partial \tilde{R}} = 0, \tag{2.51a}$$

$$\tilde{R} \to \infty, Z > 0: \quad W_1 \to 0, \quad \Theta_1 \to 0, \tag{2.52a}$$

$$\int_0^{\infty} \tilde{R} W_1 \mathrm{d}\tilde{R} = \frac{c_w}{16} Re\, Z, \tag{2.53a}$$

$$\int_0^{\infty} \tilde{R}\Theta_1 \mathrm{d}\tilde{R} = \frac{\Omega}{2\pi} Z. \tag{2.54a}$$

This set of equations (2.48)–(2.54) can be solved analytically by introducing the similarity variable

$$\eta = \frac{\tilde{X}}{\sqrt{Z}}, \quad \eta = \frac{\tilde{R}}{\sqrt{Z}}. \tag{2.55p, a}$$

Using η the solution is

$$U_1 = -\frac{c_w\sqrt{Re}}{8\sqrt{\pi}\sqrt{Z}}\eta \exp(-\tfrac{1}{4}\eta^2), \tag{2.56p}$$

$$W_1 = \frac{c_w\sqrt{Re}}{4\sqrt{\pi}} \exp(-\tfrac{1}{4}\eta^2), \tag{2.57p}$$

$$\Theta_1 = \frac{\Omega\sqrt{Pr}}{2\sqrt{\pi}\sqrt{Re}} \exp(-Pr\tfrac{1}{4}\eta^2); \tag{2.58p}$$

$$U_1 = -\frac{c_w Re}{64\sqrt{Z}}\eta \exp(-\tfrac{1}{4}\eta^2), \tag{2.56a}$$

$$W_1 = \frac{c_w Re}{32} \exp(-\tfrac{1}{4}\eta^2), \tag{2.57a}$$

$$\Theta_1 = \frac{\Omega Pr}{4\pi} \exp(-Pr\,\tfrac{1}{4}\eta^2). \tag{2.58a}$$

With respect to the flow field, this solution is equivalent to the results for the linearized far wake, given in the literature (e.g. Schlichting 1982; Loitsianski 1967). The temperature field within this approximation reflects the passive transport of the added heat due to diffusion and convection, based on the undisturbed, parallel flow. Of course, no coupling (via buoyancy forces) of the temperature field to the flow field is present.

At second order the equations become non-homogeneous and for the conservation equations we obtain

$$\frac{1}{\epsilon_2^2}\frac{\partial(\epsilon_2^2 W_2)}{\partial Z} - \frac{\partial^2 W_2}{\partial \tilde{X}^2} = -\frac{c_w^2 Re}{32\pi Z}\exp(-\tfrac{1}{2}\eta^2) - \frac{\Omega Gr\sqrt{Pr}\sqrt{Z}}{2\sqrt{\pi}Re^{5/2}}\exp(-Pr\tfrac{1}{4}\eta^2), \tag{2.59p}$$

$$\frac{\partial U_2}{\partial \tilde{X}} - \frac{1}{\epsilon_2^2}\frac{\partial(\epsilon_2^2 W_2)}{\partial Z} = 0, \tag{2.60p}$$

$$\frac{1}{\epsilon_2^2}\frac{\partial(\epsilon_2^2\Theta_2)}{\partial Z} - \frac{1}{Pr}\frac{\partial^2\Theta_2}{\partial \tilde{X}^2} = -\frac{c_w\Omega\sqrt{Pr}}{16\pi Z}\exp(-(1+Pr)\tfrac{1}{4}\eta^2); \tag{2.61p}$$

$$\frac{1}{\epsilon_2^2}\frac{\partial(\epsilon_2^2 W_2)}{\partial Z} - \left(\frac{\partial^2 W_2}{\partial \tilde{R}^2} + \frac{1}{\tilde{R}}\frac{\partial W_2}{\partial \tilde{R}}\right) = -\frac{c_w^2 Re^2}{1024Z}\exp(-\tfrac{1}{2}\eta^2) - \frac{\Omega Gr\,PrZ}{4\pi Re^2}\exp(-Pr\tfrac{1}{4}\eta^2), \tag{2.59a}$$

$$\frac{\partial(RU_2)}{\partial \tilde{R}} - \frac{\tilde{R}}{\epsilon_2^2}\frac{\partial(\epsilon_2^2 W_2)}{\partial Z} = 0, \tag{2.60a}$$

$$\frac{1}{\epsilon_2^2}\frac{\partial(\epsilon_2^2\Theta_2)}{\partial Z} - \frac{1}{Pr}\left(\frac{\partial^2\Theta_2}{\partial \tilde{R}^2} + \frac{1}{\tilde{R}}\frac{\partial\Theta_2}{\partial\tilde{R}}\right) = -\frac{c_w\Omega PrRe}{128\pi Z}\exp(-(1+Pr)\tfrac{1}{4}\eta^2). \tag{2.61a}$$

The corresponding boundary and integral conditions are

$$\tilde{X} = 0, Z > 0: \quad U_2 = 0, \quad \frac{\partial W_2}{\partial \tilde{X}} = 0, \quad \frac{\partial \Theta_2}{\partial \tilde{X}} = 0, \tag{2.62p}$$

$$\tilde{X} \to \pm\infty, Z > 0: \quad W_2 \to 0, \quad \Theta_2 \to 0, \tag{2.63p}$$

$$\int_{-\infty}^{\infty} W_2 \, \mathrm{d}\tilde{X} = \frac{\sqrt{2} c_w^2 Re \sqrt{Z}}{16\sqrt{\pi}} - \frac{\Omega Gr Z^2}{Re^{5/2}} - \frac{Gr \Delta m Z}{Re^2}, \tag{2.64p}$$

$$\int_{-\infty}^{\infty} \Theta_2 \, \mathrm{d}\tilde{X} = \frac{c_w \Omega \sqrt{Z}}{4\sqrt{\pi}} \sqrt{\frac{Pr}{1+Pr}}; \tag{2.65p}$$

$$\tilde{R} = 0, Z > 0: \quad U_2 = 0, \quad \frac{\partial W_2}{\partial \tilde{R}} = 0, \quad \frac{\partial \Theta_2}{\partial \tilde{R}} = 0, \tag{2.62a}$$

$$\tilde{R} \to \infty, Z > 0: \quad W_2 \to 0, \quad \Theta_2 \to 0, \tag{2.63a}$$

$$\int_0^{\infty} \tilde{R} W_2 \mathrm{d}\tilde{R} = \frac{c_w^2 Re^2 Z}{1024} - \frac{\Omega Gr Z^3}{6\pi Re^2} - \frac{Gr \Delta m Z^2}{Re^2}, \tag{2.64a}$$

$$\int_0^{\infty} \tilde{R} \Theta_2 \mathrm{d}\tilde{R} = \frac{c_w \Omega Re Z}{64\pi} \frac{Pr}{1+Pr}. \tag{2.65a}$$

Δm denotes the constant of integration, obtained by integrating the temperature field in equation (2.41). Here the integral of the buoyant forces across the entire control volume is required. Since the true temperature $\Theta(\tilde{X}, Z)$ is not known in the near field, we replace the definite integral with respect to Z in equation (2.41) by an indefinite integral.

With respect to the flow field the set of equations (2.59)–(2.65) introduces non-linearities of the convective terms and includes weak buoyant forces, resulting from the first-order temperature field. For the non-buoyant far wake flow, i.e. in the limit $Gr \to 0$, the above equations agree with the second-order expansion of Goldstein (1933). The convective heat transport within this approximation is based on the first-order wake velocity profiles and, hence, the buoyant contribution to the flow field does not yet influence the heat transport.

We transform the set of equations (2.59)–(2.65) to a corresponding set of ordinary differential equations by means of the similarity transformation

$$U_2 = \frac{\sqrt{2} c_w^2 Re}{16\sqrt{\pi}\sqrt{Z}} G(\eta) + \frac{\Omega Gr Z}{Re^{5/2}} I(\eta) + \frac{Gr \Delta m}{4\sqrt{\pi} Re^2} \eta \exp(-\tfrac{1}{4}\eta^2), \tag{2.66p}$$

$$W_2 = \frac{\sqrt{2} c_w^2 Re}{16\sqrt{\pi}} F(\eta) + \frac{\Omega Gr Z^{3/2}}{Re^{5/2}} K(\eta) - \frac{Gr \Delta m \sqrt{Z}}{2\sqrt{\pi} Re^2} \exp(-\tfrac{1}{4}\eta^2), \tag{2.67p}$$

$$\Theta_2 = \frac{c_w \Omega}{4\sqrt{\pi}} \sqrt{\frac{Pr}{1+Pr}} H(\eta); \tag{2.68p}$$

$$U_2 = \frac{c_w^2 Re^2}{1024\sqrt{Z}} G(\eta) + \frac{\Omega Gr Z^{3/2}}{6\pi Re^2} I(\eta) + \frac{Gr \Delta m \sqrt{Z}}{4 Re^2} \eta \exp(-\tfrac{1}{4}\eta^2), \tag{2.66a}$$

$$W_2 = \frac{c_w^2 Re^2}{1024} F(\eta) + \frac{\Omega Gr Z^2}{6\pi Re^2} K(\eta) - \frac{Gr \Delta m Z}{2 Re^2} \exp(-\tfrac{1}{4}\eta^2), \tag{2.67a}$$

$$\Theta_2 = \frac{c_w \Omega Re}{64\pi} \frac{Pr}{1+Pr} H(\eta). \tag{2.68a}$$

This generalized transformation leads to a set of ordinary differential equations for the shape functions $G(\eta), I(\eta), F(\eta), K(\eta), H(\eta)$, which is readily inferred to be

$$F'' + \tfrac{1}{2}\eta F' + F = \frac{1}{\sqrt{8\pi}} \exp(-\tfrac{1}{2}\eta^2), \tag{2.69p}$$

$$K'' + \tfrac{1}{2}\eta K' - \tfrac{1}{2}K = \frac{\sqrt{Pr}}{2\sqrt{\pi}} \exp(-Pr\,\tfrac{1}{4}\eta^2), \tag{2.70p}$$

$$G' + \tfrac{1}{2}\eta F' + F = 0, \tag{2.71p}$$

$$I' + \tfrac{1}{2}\eta K' - \tfrac{1}{2}K = 0, \tag{2.72p}$$

$$H'' + Pr\tfrac{1}{2}\eta H' + PrH = \frac{Pr\sqrt{1+Pr}}{4\sqrt{\pi}} \exp(-(1+Pr)\tfrac{1}{4}\eta^2); \tag{2.73p}$$

$$F'' + (\tfrac{1}{2}\eta + (1/\eta))F' + 2F = \exp(-\tfrac{1}{2}\eta^2), \tag{2.69a}$$

$$K'' + (\tfrac{1}{2}\eta + (1/\eta))K' = \exp(-Pr\,\tfrac{1}{4}\eta^2), \tag{2.70a}$$

$$G' + (1/\eta)G + \tfrac{1}{2}\eta F' + 2F = 0, \tag{2.71a}$$

$$I' + (1/\eta)I + \tfrac{1}{2}\eta K' = 0, \tag{2.72a}$$

$$H'' + (Pr\,\tfrac{1}{2}\eta + (1/\eta))H' + 2Pr\,H = \tfrac{1}{2}Pr\,(1+Pr)\exp(-(1+Pr)\tfrac{1}{4}\eta^2). \tag{2.73a}$$

The corresponding boundary and integral conditions are

$$\eta = 0: \quad I = 0, \quad G = 0, \quad F' = 0, \quad K' = 0, \quad H' = 0, \tag{2.74}$$

$$\eta \to \pm\infty: \quad F \to 0, \quad K \to 0, \quad H \to 0, \tag{2.75}$$

$$\int_{-\infty}^{\infty} F\,\mathrm{d}\eta = 1, \tag{2.76p}$$

$$\int_{-\infty}^{\infty} K\,\mathrm{d}\eta = -1, \tag{2.77p}$$

$$\int_{-\infty}^{\infty} H\,\mathrm{d}\eta = 1; \tag{2.78p}$$

$$\int_{0}^{\infty} \eta F\,\mathrm{d}\eta = 1, \tag{2.76a}$$

$$\int_{0}^{\infty} \eta K\,\mathrm{d}\eta = -1, \tag{2.77a}$$

$$\int_{0}^{\infty} \eta H\,\mathrm{d}\eta = 1. \tag{2.78a}$$

We apply a multiple shooting method, based on a fourth-order Runge–Kutta scheme for the integration of the associated initial value problem, to solve the above

set of ordinary differential equations, and boundary and integral conditions (2.69)–(2.78). Given a solution to the shape functions, we can summarize the results for the flow and temperature fields as follows:

$$\tilde{U} = -\frac{\bar{c}_w\sqrt{Re}}{8\sqrt{\pi}Z}\eta\exp(-\tfrac{1}{4}\eta^2) + \frac{\sqrt{2}\bar{c}_w^2 Re}{16\sqrt{\pi}Z^{3/2}}G(\eta) + \frac{\Omega Gr}{Re^{5/2}}I(\eta) + \cdots, \tag{2.79p}$$

$$W = 1 - \frac{\bar{c}_w\sqrt{Re}}{4\sqrt{\pi}\sqrt{Z}}\exp(-\tfrac{1}{4}\eta^2) - \frac{\sqrt{2}\bar{c}_w^2 Re}{16\sqrt{\pi}Z}F(\eta) - \frac{\Omega Gr\sqrt{Z}}{Re^{5/2}}K(\eta) + \cdots, \tag{2.80p}$$

$$\Theta = \frac{\Omega\sqrt{Pr}}{2\sqrt{\pi}\sqrt{Re}\sqrt{Z}}\exp(-Pr\tfrac{1}{4}\eta^2) + \frac{\bar{c}_w\Omega}{4\sqrt{\pi}Z}\sqrt{\frac{Pr}{(1+Pr)}}H(\eta) + \cdots, \tag{2.81p}$$

$$\tilde{U} = -\frac{\bar{c}_w Re}{64Z^{3/2}}\eta\exp(-\tfrac{1}{4}\eta^2) + \frac{\bar{c}_w^2 Re^2}{1024Z^{5/2}}G(\eta) + \frac{\Omega Gr}{6\pi Re^2\sqrt{Z}}I(\eta) + \cdots, \tag{2.79a}$$

$$W = 1 - \frac{\bar{c}_w Re}{32Z}\exp(-\tfrac{1}{4}\eta^2) - \frac{\bar{c}_w^2 Re^2}{1024Z^2}F(\eta) - \frac{\Omega Gr}{6\pi Re^2}K(\eta) + \cdots, \tag{2.80a}$$

$$\Theta = \frac{\Omega Pr}{4\pi Z}\exp(-Pr\tfrac{1}{4}\eta^2) + \frac{\bar{c}_w\Omega Re}{64\pi Z^2}\frac{Pr}{(1+Pr)}H(\eta) + \cdots. \tag{2.81a}$$

Within equations (2.80) we have introduced an effective drag coefficient $\bar{c}_w$, defined by

$$\bar{c}_w = c_w - \frac{2Gr\,\Delta m}{Re^{5/2}}, \quad \bar{c}_w = c_w - \frac{16Gr\,\Delta m}{Re^3}. \tag{2.82p, a}$$

The effective drag coefficient $\bar{c}_w$ includes both the forced flow drag coefficient c_w of the body and the constant of integration Δm. For an isothermal flow, $\bar{c}_w = c_w$ can be inferred from equations (2.82p, a).

2.4.3. *Limitations of the model*

At this stage it seems reasonable to summarize the assumptions and limitations which restrict the range of validity of the above model. First, applying the boundary-layer approximation within the transport equations of both momentum and heat restricts the validity to large Reynolds numbers and fluids with not too small Prandtl numbers. Thus we require

$$\sqrt{Re} \gg 1, \tag{2.83}$$

$$\sqrt{PrRe} \gg 1. \tag{2.84}$$

Secondly, the far-wake approximation restricts us to large Z. To be precise, given the actual Reynolds number, we infer from the approximative solution (2.80) that the expansion holds if

$$\sqrt{Z} \gg \frac{\bar{c}_w\sqrt{Re}}{4\sqrt{\pi}}, \quad Z \gg \frac{\bar{c}_w Re}{32}, \tag{2.85p, a}$$

is fulfilled. Thirdly, we have a limitation from the assumption of a weakly heated body. The buoyant contributions in (2.80) remain small if

$$\Omega Gr \ll \frac{Re^{5/2}}{\sqrt{Z}}, \quad \Omega Gr \ll 6\pi Re^2, \tag{2.86p, a}$$

holds.

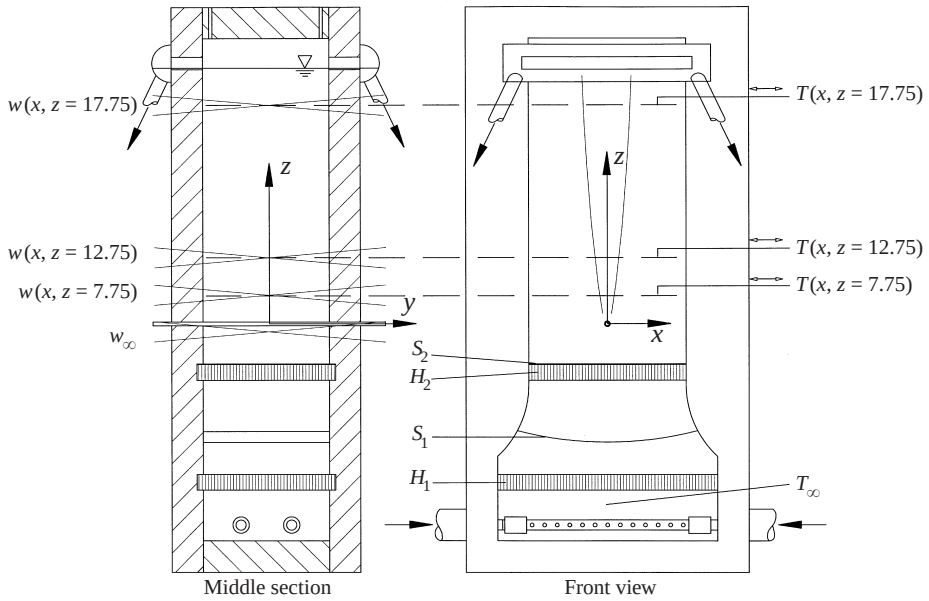

FIGURE 3. Sketch of the test section and measuring technique (approximately to scale). Measuring planes are given by dashed horizontal lines, temperature probes are shown in the front view, LDA measurement volumes are given in the middle section by cross-hairs.

Conditions (2.83), (2.84) are immediately transparent. Conditions (2.85), (2.86) *per se* are likewise physically clear as weak buoyant effects are considered. However, the combined application of conditions (2.85*p*) and (2.86*p*) for the plane problem gives

$$\frac{\bar{c}_w\sqrt{Re}}{4\sqrt{\pi}} \ll \sqrt{Z} \ll \frac{Re^{5/2}}{\Omega Gr}. \tag{2.87p}$$

This is different from the axisymmetric problem, where Z is allowed in a range

$$\frac{\bar{c}_w Re}{32} \ll Z \ll \infty. \tag{2.87a}$$

In particular condition (2.87*p*) is an unexpected result, which is caused by the growth of the buoyant term downstream for the plane case (cf. equation (2.80*p*)).

3. Experimental method

We aim to assess experimental data for the laminar mixed-convective flow in the wake of a heated body. We restrict our experiment to a heated cylinder and realize a plane flow and temperature field in the wake above this cylinder. We therefore have to establish a homogeneous laminar flow, rising in a vertical channel. This flow has to be controlled carefully with respect to flow rate and temperature. Furthermore we have to control the temperature of the cylinder. The measuring technique has to monitor the flow and temperature fields in the wake above the cylinder to allow a quantitative comparison of the experimental situation and the theoretical predictions. Based on these constraints, we have designed the following experimental setup.

3.1. *Setup and measuring technique*

The test section is sketched in figure 3. Water enters the test channel at a well-controlled temperature T_∞ from below via two horizontal pipes, which are perforated

to allow a horizontal outlet, homogeneously into the lowest chamber. Through a sequence of two honeycomb inserts (H_1, H_2) and two fine screens (S_1, S_2), in conjunction with the contraction (cf. figure 3), the flow is made parallel, and fairly uniform velocity profiles across most of the channels cross-section are obtained. The contraction serves to reduce the build-up of wall boundary layers in the lower section. Leaving the upper screen S_2, the flow passes the cylinder of diameter $d = 6\,\text{mm}$. The channel in that region has parallel walls and a square cross-section of $30 \times 30\,\text{cm}$. The water leaves the channel after a length of about 50 cm via a free interface outflow. A constant integral flow rate through the test channel and a constant entrance temperature of the water is achieved by a controlled pump, complete insulation of the test channel and all elements of the water circuit and two heat exchangers, which have an extremely carefully controlled temperature at their secondary side. This keeps the velocity w_∞ upstream of the cylinder constant to $\pm 1\%$ and the inlet temperature T_∞ constant to $\pm 0.05\,^\circ\text{C}$. The cylinder is likewise kept at constant temperature T_b. This is achieved by circulating water of constant temperature through a copper pipe of 6 mm outer diameter, which gives a temperature constancy of about $\pm 0.02\,^\circ\text{C}$.

The measuring system consists of a number of thermocouples mounted on traversing drives, which allow the measurement of temperature profiles $T_i(x)$ at three distances z_1, z_2, z_3 above the cylinder. On a dimensionless scale, these planes are located at $Z_i = 7.75, 12.75, 17.75$. The temperature profiles $T_i(x)$ are taken in the middle of the channel, where an almost undisturbed plane flow is present. Moreover, the homogenity of temperature T_∞ in the plane of the upper screen S_2 is monitored by another three thermocouples at different positions. All temperature measurements are taken as the difference to the inlet temperature T_∞, which is taken within a copper cube of 3 cm side length positioned within the lowest chamber. Additionally three PT100 resistant thermometers monitor at higher accuracy the cylinder temperature at two positions and also the inlet temperature T_∞. Accuracy of the thermocouple difference measurements is $\pm 0.05\,^\circ\text{C}$, while the PT100 probes are typically accurate to $\pm 0.01\,^\circ\text{C}$.

The flow field is measured using two one-component laser Doppler anemometers (LDA). The first LDA measuring volume is at a fixed point $(X, Z) = (10, -5)$ upstream of the cylinder. This position provides an accurate measurement of the forced flow velocity w_∞ hardly affected by the presence of the cylinder. The signals are extracted from the forward scattered light. The second LDA has a relatively small optical head connected via fibre optics to a stationary unit with laser, Bragg cell, photomultipliers, etc. Its measuring volume is traversed along identical lines as the thermocouples by means of another stepping motor drive. The orientation is such that profiles $w_i(x)$ are measured at three distances z_1, z_2, z_3 above the cylinder, while in this case the backscattered light is picked up by the optical head. Likewise these velocity profiles are taken in the middle of the channel to focus mainly on plane effects. The precision of both LDA measuring systems, due to a sophisticated transient recorder-based evaluation of the signals, should be in the range $\pm 0.2\,\text{mm}\,\text{s}^{-1}$, the positioning of traversing drives (velocity and temperature probes) is highly accurate to $\pm 0.01\,\text{mm}$. Typically, profiles of temperature and velocity are taken in steps down to $\Delta x = 1\,\text{mm}$.

3.2. *Scaling and preliminary measurements*

In order to apply the asymptotic model to the experimental conditions we need to determine several (integral) parameters, namely the dimensionless groups $Re, c_w, \bar{c}_w, Gr, \Omega, Pr$. Moreover, the quantities in the scaling relations (2.8)–(2.11) w_∞, T_b, T_∞ need to be determined. The temperatures T_b and T_∞ of the cylinder and of the fluid upstream

Property	Symbol	Value	Units
density	ρ_∞	9.9705×10^2	$\mathrm{kg\,m^{-3}}$
specific heat	c_p	4.1790×10^3	$\mathrm{Ws\,kg^{-1}\,K^{-1}}$
thermal expansion	α	2.5720×10^{-4}	$\mathrm{K^{-1}}$
heat conductivity	λ	6.0720×10^{-5}	$\mathrm{W\,m^{-1}\,K^{-1}}$
viscosity	ν	8.9300×10^{-7}	$\mathrm{m^2\,s^{-1}}$

TABLE 1. Properties of the test liquid (water) for $T_0 = 25\,^\circ\mathrm{C}$, $p_0 = 1$ bar (from Weast 1980).

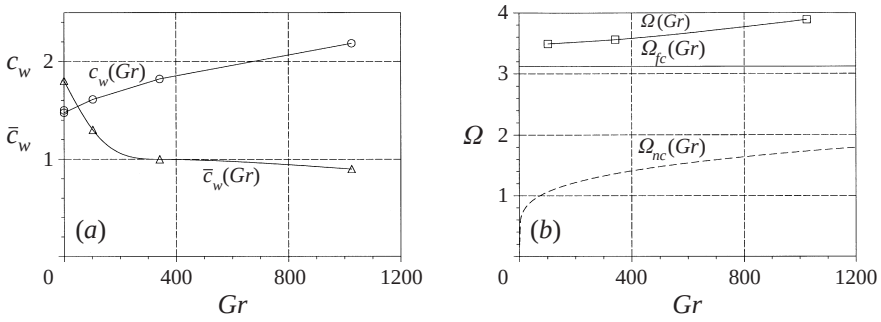

FIGURE 4. Drag coefficient c_w, effective drag coefficient $\bar{c}_w$ and heat transfer coefficient Ω as function of Gr.

are directly available from measurements. Thus, as T_∞ is kept at 25 °C, all liquid properties $\rho_\infty, c_p, \alpha, \lambda, \nu$ are known. These properties are summarized in table 1. The velocity w_∞ is directly measured by the stationary LDA system. As the cross-section of the channel is finite, the no-slip condition leads to the development of kinematic boundary layers at all four vertical walls downstream of the last screen insert S_2. For reasons of continuity, the presence of low-velocity regions at the walls causes increased velocity amplitudes in the intermediate region between the wake and the wall boundary layers. As the wall boundary layers increase in thickness downstream, an acceleration of the flow in the intermediate region is the consequence. Thus, in the measuring planes $Z_i = 7.75, 12.75, 17.75$ we expect $w_{\infty,i} > w_\infty$ in the outer region. In fact, we find due to these sidewall boundary layers an increase of w_∞ by about 18% along the channel. For scaling of the velocity profiles we therefore use the spatially averaged plateau value $w_{\infty,i}$ in the outer region of the respective plane Z_i, which typically occurs in a region $|X| > 4$. For the determination of the Reynolds number Re (cf. (2.19)), in contrast, we use an averaged value from the planes $Z = -5$ and $Z = 17.75$.

The drag coefficient c_w of the cylinder for forced flow conditions depends purely on the Reynolds number Re. Schlichting (1982) gives for the experimental Reynolds number $Re = 39.4$ a value of $c_w = 1.8$. It is alternatively possible to use our numerical (FEM) results to determine c_w. Depending on the method of determination (cf. § 2.3), we find $c_w = 1.475, 1.499$. All values are given in figure 4(a) for $Gr = 0$.

For mixed-convection conditions we use an integration of the stress field around the cylinder contour to determine the force, and thus c_w, acting on the heated cylinder ($Gr > 0$). Using this method we find increasing values of c_w for increasing Grashof numbers Gr (cf. circles in figure 4a). An inspection of the flow field reveals that this increase of drag is due to the disappearance of the recirculation zone behind

the cylinder. Thus, for large Grashof numbers, the flow is attached to the complete cylinder contour and a stronger interaction occurs.

As inferred in § 2.4.2, the asymptotic model is based on an effective drag coefficient $\bar{c}_w$, defined by equation (2.82*p*). The constant of integration Δm in equation (2.82*p*) is constant with respect to the spatial coordinates $\tilde{X}, Z, \eta$. The values of $\bar{c}_w$ employed in the asymptotic model for different Grashof numbers are given in figure 4(*a*) as triangles. These values are inferred from the corresponding FEM simulations. For small Grashof numbers a linear decrease of $\bar{c}_w$ with increasing Gr can be seen, precisely as predicted by equation (2.82*p*). The departure from the linear behaviour for large Gr is not surprising, as Δm develops a dependence on Gr.

The Prandtl number Pr is available from the fluid properties given in table 1. For the reference temperature $T_\infty = 25\,^\circ\mathrm{C}$ we find $Pr = 6.128$. Within the asymptotic model the heat input is included in the parameters Gr and Ω. The Grashof number is readily computed from the fluid properties and the measured temperatures T_b, T_∞. The dimensionless heat transfer coefficient Ω is linked to the Nusselt number Nu and quantifies the integral heat transfer. We use our numerical (FEM) results to determine the transferred heat $\dot{q}$ (cf. § 2.3) and, hence, Ω via equation (2.42*p*). The values of Ω obtained for various Grashof numbers are plotted in figure 4(*b*) as squares. An increase of Ω with increasing Gr is obvious. We check these heat transfer data by using literature correlations for the forced flow and natural convective flow heat transfer from a cylinder. Following Gnielinski (1975) and Churchill & Chu (1975) for laminar flow the empirical correlations

$$\Omega_{fc} = 2NuPr^{-1} = 1.6644Re^{1/2}Pr^{-2/3}, \tag{3.1}$$

$$\Omega_{nc} = 2NuPr^{-1} = 2Pr\left[0.6 + \frac{0.387(PrGr)^{1/6}}{\left(1 + (0.559/Pr)^{9/16}\right)^{8/27}}\right]^2, \tag{3.2}$$

hold. For the specific Reynolds and Prandtl numbers in the experiment, $Re = 39.4, Pr = 6.128$, the correlations yield

$$\Omega_{fc} = 3.12, \tag{3.3}$$

$$\Omega_{nc} = (0.43 + 0.279Gr^{1/6})^2. \tag{3.4}$$

The Nusselt number in equations (3.1), (3.2) is defined by

$$Nu = \frac{\pi}{2}\frac{hd}{\lambda}, \tag{3.5}$$

where h is the heat transfer coefficient. Both Ω_{fc} and Ω_{nc} are given in figure 4(*b*) by solid and dashed lines. Our results from the FEM simulations for Ω (cf. squares in figure 4*b*) compare reasonably well with the correlations (3.3), (3.4). First, the value Ω_{fc} is about 10% lower than the extrapolated value for $Gr \to 0$ from our data. Secondly, the increase of Ω with increasing Gr occurs perfectly parallel to the increase of Ω_{nc} in correlation (3.4). However, the curve $\Omega_{nc}(Gr)$ is shifted to lower values. This is due to the presence of the forced flow within the present heat transfer data in figure 4*b* (squares). A summary of the experiments presented is given in table 2.

4. Results

In the following sections we shall give results obtained for the flow field in various parameter regimes. As only plane experiments have been performed, we restrict the

$\overline{w}_\infty$ (m s^{-1})	Re	$(T_b - T_\infty)$ (°C)	Gr
5.864×10^{-3}	39.4	0.0	0.0
5.864×10^{-3}	39.4	0.15	102.5
5.864×10^{-3}	39.4	0.50	341.7
5.864×10^{-3}	39.4	1.50	1025.1

TABLE 2. Summary of experiments ($T_0 = T_\infty = 25\,°\mathrm{C}$).

discussion to the plane problem. We focus on the dimensionless vertical velocity profiles $W(X, Z_i)$ in three different planes downstream, above the cylinder. Temperature profiles $\Theta(X, Z_i)$ of reasonable quality have been measured only for the strongly heated cylinder (§ 4.3) and they are discussed only in that section.

The isothermal problem (§ 4.1) is discussed to check the consistency of the results from the experiments, the asymptotic model and the numerical (FEM) simulations. Here, the particular aspects of the forced flow can be verified, such as the development of the far (and near) wake. This part does not contain new results, as all features of far wakes presented here are well known from the literature (e.g. Berger 1971). Section 4.2 relates to the weakly heated cylinder and in particular verifies aspects of weak buoyant forces within the asymptotic model. Here the parameters are chosen such that the asymptotic model applies. Section 4.3, finally, relates to the strongly heated cylinder and gives results for parameter ranges outside the validity of the asymptotic model. Here, mixed convection with strong buoyant forces is present, and only a comparison of experimental findings and numerical (FEM) simulations is reasonable.

4.1. *Isothermal wake*

In figure 5 our results for the flow field are collated for an isothermal situation. We give in figure 5(*a*) measured vertical velocity profiles $W(X, Z_i)$ in three planes Z_i above the cylinder. The data points are shown on both sides of the symmetry line $X = 0$ in addition to least-square fits of the symmetric form

$$W = 1 - C_1 \exp(C_2 X^2). \tag{4.1}$$

We see in the plane $Z = 7.75$ (symbols ∇) a pronounced wake profile with a substantial velocity deficit on the centreline $X = 0$. As we move downstream to $Z = 12.75, 17.75$ (symbols $\square, \bigcirc$) the velocity deficit decreases. Moreover, the width of the wake (in X) increases downstream. Employing equation (2.85*p*) we can estimate the small parameter in the asymptotic representation to be

$$\frac{\bar{c}_w \sqrt{Re}}{4\sqrt{\pi}\sqrt{Z_i}} = 0.57, 0.45, 0.38, \tag{4.2}$$

for the planes $Z_i = 7.75,\ 12.75,\ 17.75$. Thus, particularly for Z_1, the asymptotic representation may be critical.

Figure 5(*c*) shows the corresponding profiles obtained by means of the numerical (FEM) simulations. Here, the same features of the wake are observed, namely a widening and a filling up of the wake profile with increasing Z. Quantitatively, two characteristic differences arise in comparison with the experimental profiles in figure 5(*a*). First, the numerical simulations give velocities $W > 1$ outside the wake. In contrast, the experimental profiles give $W \leqslant 1$ in the outer region. This discrepancy

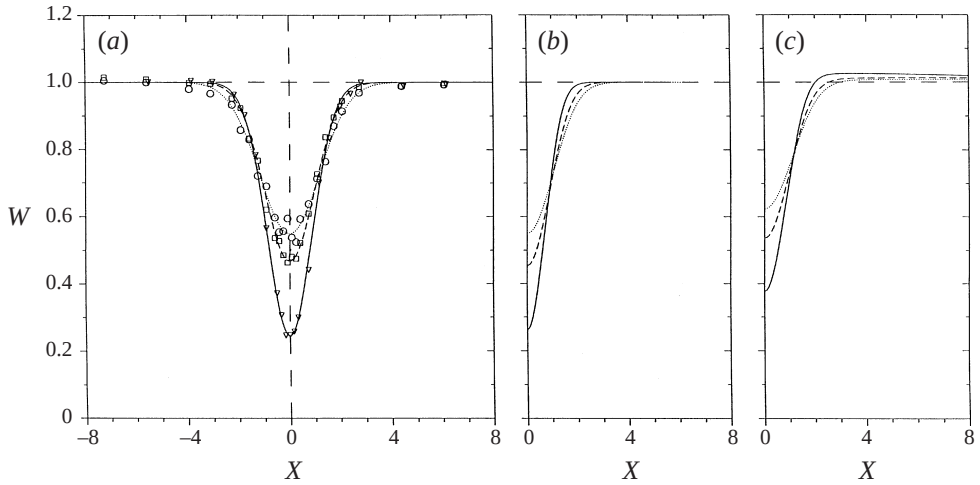

FIGURE 5. Profiles of the dimensionless vertical velocity $W(X, Z_i)$ downstream of an isothermal cylinder: (*a*) the experimental data and corresponding least-square fits, (*b*) results from the asymptotic theory and (*c*) results from the numerical simulations. The distances above the cylinder are $Z_i = 7.75$ (∇, ———), 12.75 ($\square$, — — —), 17.75 ($\bigcirc$, · · · · · ·), the parameters are $Re = 39.4, c_w = \bar{c}_w = 1.8$.

arises from the different methods of scaling. In the numerical simulations we force $W = 1$ at the inflow boundary and $W_\infty \to 1$ is obtained at the side boundary for large X. The flow field outside the wake region thus has velocity amplitudes $W > 1$ for reasons of continuity. In the experiments the velocity w_∞ for $x \to \infty$ is not accessible, since the channel has a finite width in both horizontal directions. Therefore, w_∞ is taken from the plateau of the measured profiles $w(x, z_i)$, which typically occurs in a region $|X| > 4$. By scaling with the averaged plateau value, all experimental profiles approach $W_\infty = 1$ outside the wake region. This discrepancy, therefore, is an artifact of the scaling methods.

Secondly, the velocity deficit in the centre of the wake ($X = 0$) from the numerical simulation is smaller by about 12% than the experimental findings. This is a consequence of the non-perfect experimental conditions. While the numerical and asymptotical results are obtained for a perfectly two-dimensional situation, the experimental results are affected to some degree by the presence of the walls. In the experiment we have a slight acceleration of the forced flow in the outer region and not a perfectly constant w_∞. These experimental imperfections are outlined in § 3.2 in some detail. In fact, three-dimensional numerical simulations have shown that this discrepancy with respect to the wake amplitude is caused by the acceleration of the outer flow. While we have to be aware that the velocity amplitudes are not perfectly in accord, a careful analysis of the width of the wakes from both experimental measurements and numerical simulations shows excellent agreement.

The results for the vertical velocity profiles $W(X, Z_i)$ from the asymptotic model are collated in figure 5(*b*). Following Schlichting (1982), we use a drag coefficient of $c_w = 1.8$ for the Reynolds number $Re = 39.4$. We have compared our asymptotic results with the second-order expansion of Goldstein (1933), given likewise in Berger (1971). The profiles of both velocity components are identical. Moreover, we find good agreement between the asymptotic model and experimental data. The differences are less than 2.5% with respect to the amplitude, and less than 8% with respect to the width of the wake. The asymptotic theory does not take into account the displacement

effect of the cylinder as a solution for large z is inferred. This gives profiles with $W \leqslant 1$ outside the wake region. The loss of momentum due to the presence of the cylinder, on the other hand, is correctly reflected within the asymptotic model.

We find experimentally the power law

$$1 - W(0, Z) \propto Z^{-0.63} \tag{4.3}$$

for the wake amplitude. The corresponding asymptotic and numerical dependences are

$$1 - W(0, Z) \propto Z^{-0.596}, \tag{4.4}$$

$$1 - W(0, Z) \propto Z^{-0.608}. \tag{4.5}$$

In all cases the power laws give an excellent representation of the data in the complete range $7.75 \leqslant Z \leqslant 17.75$. The width of the wake δ in the following is based on the criterion

$$\frac{1 - W(\delta, Z)}{1 - W(0, Z)} = \frac{1}{100}. \tag{4.6}$$

Using least-square fits, we infer power-law dependences for $\delta(Z)$. The asymptotic and numerical results are perfectly represented by

$$\delta \propto Z^{0.478}, \tag{4.7}$$

$$\delta \propto Z^{0.461}. \tag{4.8}$$

The experimental data, in contrast, do not allow a single power-law dependence for the complete range in Z. The experimental data for $Z > 10$, though, follow closely the theoretical dependences given above. This observation indicates that the experimental wake is not self-similar in the near field, due to the finite diameter of the cylinder.

Generally, the excellent agreement between the experimental data and asymptotic model is not surprising, as the asymptotic model is based on the drag coefficient c_w. The value of c_w in the literature, of course, is inferred from careful experimental measurements (cf. Schlichting 1982).

4.2. *Weakly heated cylinder*

In this section we give two typical results for flow fields featuring weak buoyant forces. The first example is obtained for a Grashof number of $Gr = 102.5$. Employing equation (2.86*p*), we obtain for $Z_i = 7.75, 12.75, 17.75$,

$$\frac{\Omega Gr \sqrt{Z_i}}{Re^{5/2}} = 0.10, 0.13, 0.15 \ll 1. \tag{4.9}$$

Thus, the asymptotic model is valid for all Z_i.

The results for the profiles $W(X, Z_i)$ are collated in figure 6. Even though the profiles look qualitatively similar to the forced flow profiles (cf. figure 5), an inspection of the amplitudes in figure 6(*a*) reveals that buoyant forces have accelerated the flow in the wake centre. Given identical Reynolds numbers ($Re = 39.4$), the measured profiles for forced flow give values of $W(0, 7.75) \simeq 0.24$ on the centreline. For the weak buoyant flow ($Gr = 102.5$) we find, in contrast, $W(0, 7.75) \simeq 0.52$. The velocity deficit in the wake centre, thus, is considerably reduced.

In figure 6(*a*) the measured data from the corresponding experiments are plotted as symbols and least-square fits of the symmetric form

$$W(X, Z) = 1 - C_1 \exp(C_2 X^2) + C_3 \exp(C_4 X^2) \tag{4.10}$$

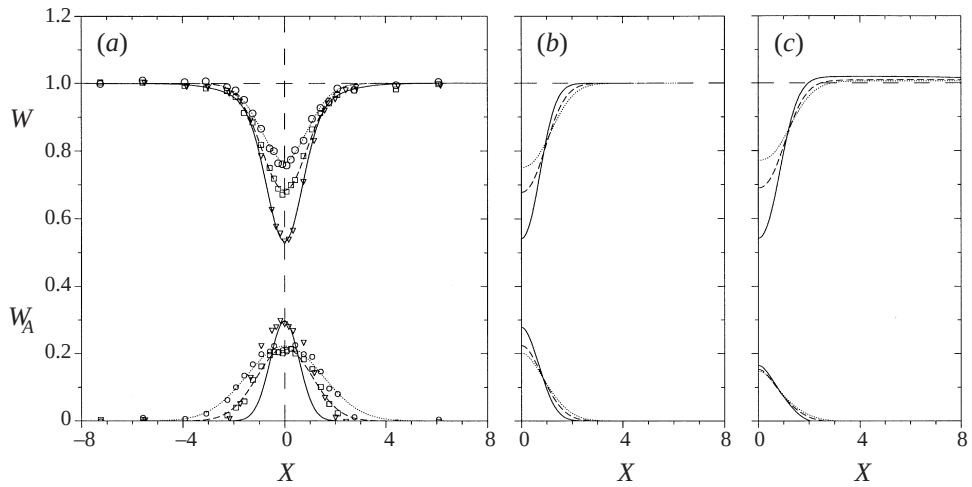

FIGURE 6. Profiles of the dimensionless vertical velocity $W(X, Z_i)$ and its buoyant contribution $W_A(X, Z_i)$ downstream of a weakly heated cylinder: (*a*) the experimental data and corresponding least-square fits, (*b*) results from the asymptotic theory and (*c*) results from the numerical simulations. The distances above the cylinder are $Z_i = 7.75$, 12.75, 17.75, the parameters are $Re = 39.4, \bar{c}_w = 1.3, Gr = 102.5, \Omega = 3.49, Pr = 6.13$. Symbols as in figure 5.

are given as lines. The form (4.10) gives a reasonably accurate fit to all experimental data and has been chosen based on the asymptotic results in equation (2.80*p*). In figure 6(*a*), in addition to the measured profiles $W(X, Z_i)$, the contribution from the buoyant forces

$$W_A(X, Z_i) = C_3 \exp(C_4 X^2) \tag{4.11}$$

is plotted. This is obtained experimentally from the difference between the profiles for $Gr = 102.5$ and the profiles for pure forced flow ($Gr = 0$). The experimental data in figure 6(*a*) suggest, first, wake-type profiles $W(X, Z_i)$, whereas the velocity deficit decreases downstream for increasing Z. Even though the data and fits indicate to some degree that the width of the wake increases downstream, a reliable statement on this question cannot be given due to the slightly scattered data. Secondly, the extracted profiles $W_A(X, Z_i)$ of the buoyant contribution have a narrow Gaussian shape at the first plane $Z_1 = 7.75$ (symbols $\triangledown$), which develops downstream into a broader shape with smaller amplitudes.

The results from the asymptotic model are given in figure 6(*b*). The overall profiles $W(X, Z_i)$ agree in both amplitude and width with the measured profiles at all locations Z_i (cf. figure 6*a*). We find differences of less than 1.7% in the amplitudes and less than 6.2% in the width of the wake. From the asymptotic profiles a definite increase of the wake width downstream can be inferred. Inspecting the buoyant contribution $W_A(X, Z_i)$, we see that the asymptotic results reasonably resemble the experimental data from figure 6(*a*). Again a Gaussian profile, which decreases in amplitude and develops a broader shape downstream, is obtained. Finally, the numerical simulation results in figure 6(*c*) agree well with both the experimental and the asymptotic results as far as the overall profiles $W(X, Z_i)$ are concerned. The buoyant contribution $W_A(X, Z_i)$, in contrast, exhibits smaller amplitudes in all planes Z_i. Moreover, the amplitudes of the buoyant contribution remain almost identical in all three planes Z_i. Here some discrepancy remains in comparison with both experimental and asymptotic findings, which both give decreasing amplitudes of the buoyant contribution

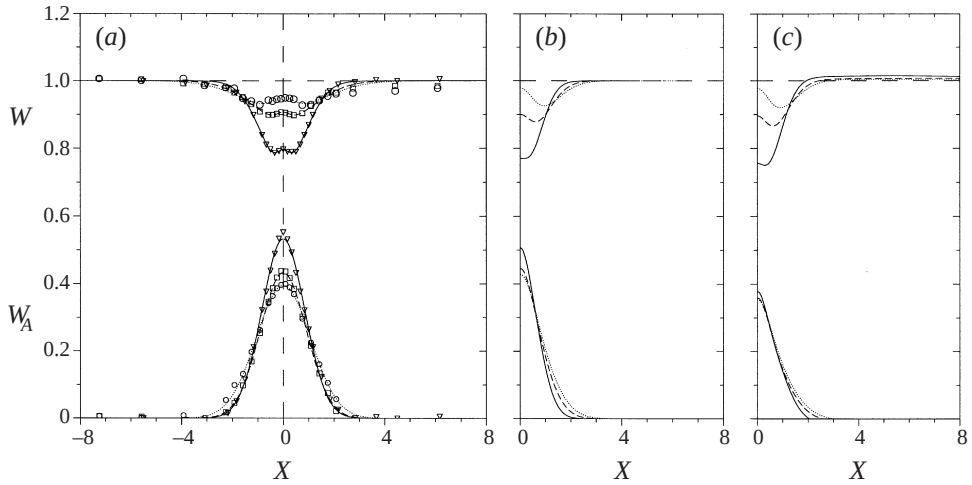

FIGURE 7. As figure 6 but for $\bar{c}_w = 1.0$, $Gr = 341.7$, $\Omega = 3.56$.

downstream. This discrepancy is a direct consequence of the numerical forced-flow results (cf. figure 5*c*). Here the velocity deficit in the wake has been underpredicted, such that the difference between forced flow profiles and weak buoyant profiles gives correspondingly poor results.

Figure 7 relates to a somewhat higher temperature of the cylinder. In this case we have a Grashof number of $Gr = 341.7$ and can already infer from the velocity profiles $W(X, Z_i)$ that buoyant forces have led to a characteristic change. From (2.86*p*) we estimate the small parameter in the asymptotic model. We find in the three planes $Z_i = 7.75, 12.75, 17.75$

$$\frac{\Omega Gr\sqrt{Z_i}}{Re^{5/2}} = 0.35, 0.45, 0.53. \tag{4.12}$$

These numbers indicate that at least for large Z_i we are at the limit of the asymptotic model, as buoyant forces develop a substantial contribution to the flow field.

We continue to discuss the experimental findings, as collated in figure 7(*a*). All measured velocity profiles $W(X, Z_i)$ indicate a pronounced buoyant acceleration of the fluid in the wake centre. The experimental observations are in good agreement with the corresponding asymptotic and numerical profiles $W(X, Z_i)$ (cf. figures 7*b*, 7*c*). This indicates that the asymptotic model remains perfectly valid even for this large Grashof number of $Gr = 341.7$. In addition to the velocity amplitudes, the total width of the wake and the width of the inner buoyant zone are predicted correctly, both by the asymptotic model and the numerical simulation. If we focus on the buoyant contribution $W_A(X, Z_i)$, we consistently find in all profiles a decrease of the amplitudes and an increase of the width of the buoyant zone downstream. The amplitudes of $W_A(X, Z_i)$ from the numerical simulation again have some discrepancies with the experimental amplitudes in figure 7(*a*). The reason for these discrepancies has already been outlined above.

4.3. *Strongly heated cylinder*

In figure 8 we have collated velocity profiles obtained for a large Grashof number of $Gr = 1025.1$. For such a high cylinder temperature the hot fluid in the wake develops strong buoyant forces, comparable to inertial forces. This can be checked via relation

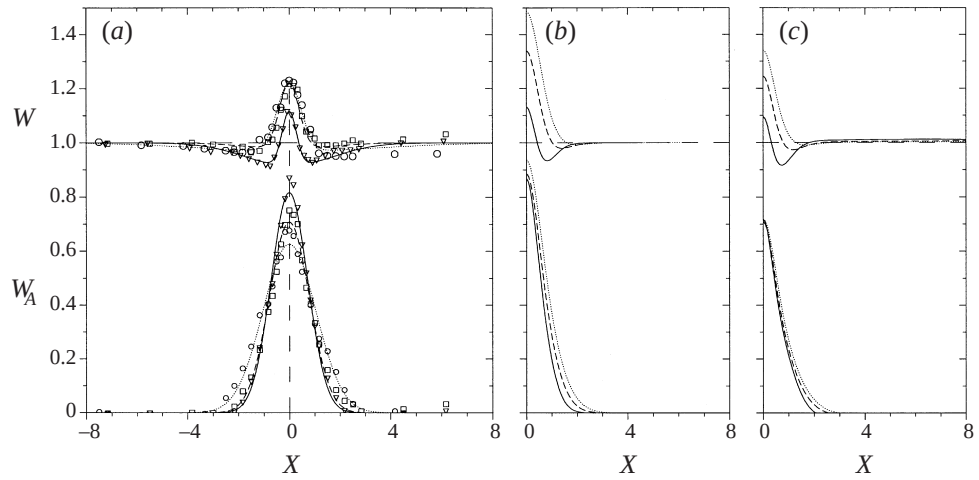

FIGURE 8. Profiles of the dimensionless vertical velocity $W(X, Z_i)$ and its buoyant contribution $W_A(X, Z_i)$ downstream of a strongly heated cylinder: (*a*) the experimental data and corresponding least-square fits, (*b*) results from the asymptotic theory and (*c*) results from the numerical simulations. The distances above the cylinder are $Z_i = 7.75, 12.75, 17.75$, the parameters are $Re = 39.4, \bar{c}_w = 0.9, Gr = 1025.1, \Omega = 3.89, Pr = 6.13$. Symbols as in figure 5.

(2.86*p*), which gives in the three planes $Z_i = 7.75, 12.75, 17.75$

$$\frac{\Omega Gr\sqrt{Z_i}}{Re^{5/2}} = 1.14, 1.46, 1.72. \tag{4.13}$$

Clearly, within this range of parameters the asymptotic model is not expected to be valid. Therefore, only a comparison of experimental and numerical (FEM) data is reasonable.

The experimental velocity profiles $W(X, Z_i)$ in figure 8(*a*) show a discernible wake contribution only in the first plane $Z_1 = 7.75$ (symbols $\triangle$). The profiles further downstream ($Z_2 = 12.75$, $Z_3 = 17.75$) are dominated by strong buoyant plumes in the centre which have centreline velocities $W(0, Z) > 1$, exceeding the free-stream velocity $W_\infty = 1$. An inspection of the buoyant contribution $W_A(X, Z_i)$ reveals, in accord with the weakly heated cases, a narrow Gaussian profile with decreasing centre amplitude and increasing width downstream. The asymptotic model (figure 8*b*) fails to predict these profiles at a reasonable accuracy. First, the overall profiles $W(X, Z_i)$ exhibit far too high amplitudes in the centre. Secondly, the buoyant contribution $W_A(X, Z_i)$ in figure 8(*b*) shows even increasing amplitudes downstream. This is qualitatively in contradiction with the experimental findings in figure 8(*a*). The widening of the Gaussian profile $W_A(X, Z_i)$ from the experiment and asymptotic model, though, happens to be in agreement. To summarize, the asymptotic model for large Gr, outside its range of validity, overpredicts the buoyant effects.

The results from the corresponding numerical simulation are collated in figure 8(*c*). The overall velocity profiles $W(X, Z_i)$ show a reasonable agreement with the experimental data in figure 8(*a*). The acceleration of the flow in the centre as one moves downstream, though, is slightly overpredicted by the numerical simulation. The buoyant contribution $W_A(X, Z_i)$ reveals a Gaussian profile of constant centre amplitude (in Z), which becomes broader downstream. Once more, there remains a discrepancy with respect to the amplitude $W_A(0, Z_i)$: the experiment indicates a distinct decrease of the centre amplitude downstream.

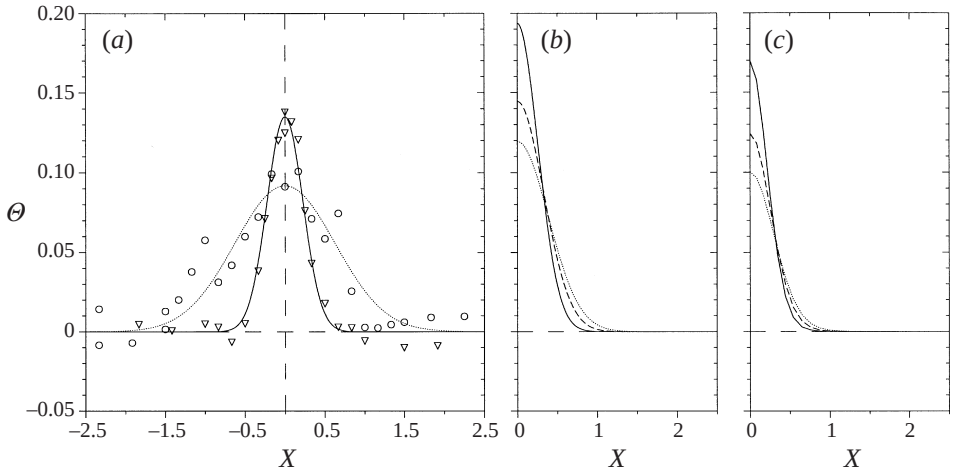

FIGURE 9. Profiles of the dimensionless temperature $\Theta(X, Z_i)$ downstream of a strongly heated cylinder: (*a*) the experimental data and corresponding least-square fits for Z_1 (○), Z_3 (△); (*b*) results from the asymptotic theory and (*c*) results from the numerical simulations. The distances above the cylinder are $Z_i = 7.75, 12.75, 17.75$, the parameters are $Re = 39.4, \bar{c}_w = 0.9, Gr = 1025.1, \Omega = 3.89, Pr = 6.13$. Line styles in (a, b, c) as in figure 5.

As mentioned above, temperature profiles $\Theta(X, Z_i)$ have been measured in the experiments at much lower accuracy. This is due, first, to a temperature increase of always less than 0.2 K in the first measuring plane and even smaller temperature amplitudes in the measuring planes downstream. Secondly, for high cylinder temperatures the situation is not perfectly stationary, leading to further errors from time-averaging. Nevertheless, it is useful to compare temperature profiles for the strongly heated cylinder at least. The data are collated in figure 9. The experimental data are given in figure 9(*a*) for two planes, namely $Z_1 = 7.75$, $Z_3 = 17.75$, in form of the symbols ○ and △. Moreover, least-square fits of the form

$$\Theta = C_1 \exp C_2 X^2 \tag{4.14}$$

are given by the solid and dotted lines. The profiles are of Gaussian type, whereas the temperature in the centre $\Theta(0, Z_i)$ decreases downstream and the width of the heated zone δ_{th} increases downstream. A qualitatively identical behaviour can be seen in the numerical simulation profiles in figure 9(*c*). Quantitatively, however, the peak temperatures $\Theta(0, Z_i)$ from the numerical simulation are somewhat higher. Furthermore, the widening of the heated zone δ_{th} downstream appears more pronounced in the experimental data. This discrepancy is presumably caused by slight temporal oscillations downstream of the cylinder in the experiment. These oscillations appear to be precursors of an instability leading to a time-dependent wake further downstream. This causes a more effective transport of momentum and heat in the horizontal direction X. Moreover, the time-averaging during the temperature measurements for time-dependent wakes leads to a smearing of the profiles.

Finally, the temperature profiles from the asymptotic model in figure 9(*b*) dramatically overestimate the peak temperature $\Theta(0, Z_i)$. Moreover, the width development is not in accord with the experimental data. This is not surprising, as equation (4.13) proves that this model is outside of its range of validity.

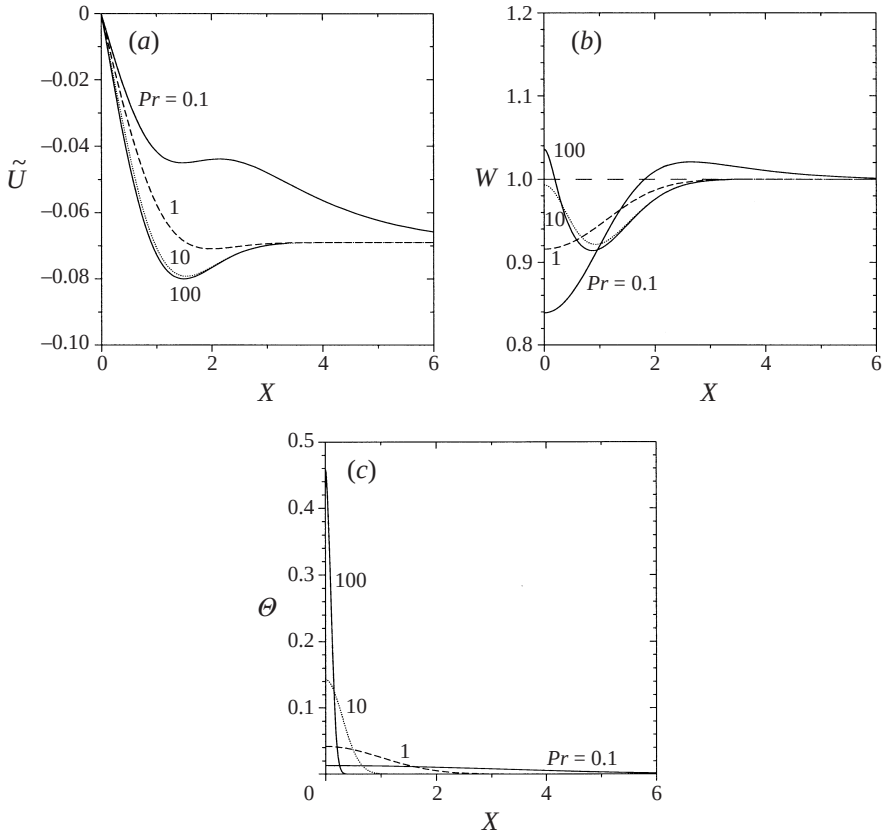

FIGURE 10. Profiles of (*a*) the dimensionless horizontal velocity $\tilde{U}(X, Z_3)$, (*b*) the dimensionless vertical velocity $W(X, Z_3)$, (*c*) the dimensionless temperature $\Theta(X, Z_3)$ downstream of a weakly heated body. The distance above the body is $Z_3 = 17.75$, the parameters are $Re = 39.4, \bar{c}_w = 1.0, Gr = 341.7, \Omega = 3.56$.

4.4. *Effect of Prandtl number*

We now discuss the influence of the Prandtl number, or in physical terms of the fluid properties, on the flow and temperature fields. In §§ 4.1–4.3 we have verified the asymptotic model against both experimental and numerical (FEM) findings. Thus, this discussion is purely based on the asymptotic model, within its range of validity (cf. § 2.4.3). Moreover, we focus on the plane problem.

In figure 10 we collate a set of results, obtained for Prandtl numbers in the range $0.1 \leqslant Pr \leqslant 100$. The results are obtained for mixed-convective conditions and a weakly heated body, i.e. the parameters are $Re = 39.4, Gr = 341.7$. The profiles are taken at a distance $Z_3 = 17.75$ downstream of the body. From the temperature profiles $\Theta(X, Z_3)$ in figure 10(*c*) the influence of the Prandtl number can be inferred. For a large Prandtl number of $Pr = 100$ we have a poorly conducting fluid, causing a narrow heated zone of thickness $\delta_{th} \simeq 0.3$. In contrast, a small Prandtl number of $Pr = 0.1$, due to good conduction in the fluid, leads to a wide heated zone of thickness $\delta_{th} \simeq 9$. The thickness of the heated zone is defined by

$$\frac{\Theta(\delta_{th}, Z_i)}{\Theta(0, Z_i)} = \frac{1}{100}. \tag{4.15}$$

Similarly, the amplitude $\Theta(0, Z_3)$ of the Gaussian-type profiles is strongly dependent on the Prandtl number. Here we find an increase of the centre temperature $\Theta(0, Z_3)$ with increasing Prandtl number. A careful analysis of all data reveals that both the width of the heated zone δ_{th} and the centre temperature $\Theta(0, Z)$ follow a power law in the range investigated, $5 \leqslant Z \leqslant 20$. For the complete range of Prandtl numbers $0.1 \leqslant Pr \leqslant 100$ we find the behaviour

$$\delta_{th} \propto Pr^{-0.504}, \tag{4.16}$$

$$\Theta(0, Z) \propto Pr^{0.523}. \tag{4.17}$$

The power law behaviour (4.16), (4.17) of both quantities can similarly be found from the leading-order term in equation (2.81*p*). The second-order term in equation (2.81*p*) does not change this behaviour significantly.

Depending on the temperature field, the buoyant forces will either be concentrated in the centre (cf. $Pr = 100$), or will be distributed over a wide range (cf. $Pr = 0.1$). The vertical velocity profiles $W(X, Z_3)$ in figure 10(*b*) reflect this, as for $Pr = 100$ the fluid is accelerated to velocities $W(0, Z_3) \geqslant 1$ in a narrow centre zone. For $Pr = 0.1$, in contrast, a wide range of fluid inside and outside the wake experiences buoyant forces and, thus, only weak acceleration. For $Pr = 1$ we find the width of the heated zone δ_{th} and the width of the wake δ, defined by equation (4.6), to be equal, i.e. $\delta \simeq \delta_{th} \simeq 3$. The width of the kinematic wake δ remains independent of Prandtl number. The behaviour of the centre amplitude $W(0, Z)$ has likewise been analysed with respect to a power-law behaviour. Here, only in the limited range $0.1 \leqslant Pr \leqslant 10$, can the data be approximated by the power law

$$W(0, Z) \propto Pr^{0.032}. \tag{4.18}$$

For $Pr > 10$ the amplitudes $W(0, Z)$ asymptotically approach a constant value for $Pr \to \infty$ in all planes Z_i. Physically this is expected, since even temperature profiles in the form of a delta-function (for $Pr \to \infty$) due to viscous effects lead to buoyant plumes of finite width and, hence, finite amplitude.

The horizontal velocity profiles $\tilde{U}(X, Z_3)$ in figure 10(*a*) in all cases show transport of fluid from the far-outside region into the wake. The maximum amplitude of $\tilde{U}(X, Z_3)$ occurs for $Pr = 100$ at a position $X \simeq 1.5$. The curve for $Pr \to \infty$, in fact, cannot be distinguished from the curve obtained for $Pr = 100$. For smaller Prandtl numbers the amplitude of $\tilde{U}(X, Z_3)$ in the intermediate region decreases. The amplitude of $\tilde{U}(X \to \infty, Z_3)$ in the far-outside region, on the other hand, is not dependent on Pr.

4.5. *Effect of Grashof number*

The Grashof number, or in physical terms the body temperature, is a further interesting parameter. This discussion, once more, is for the plane problem, based on the asymptotic model. Even though the above verification of the asymptotic model is performed for a heated body ($Gr \geqslant 0$), we extend the discussion to a cooled body ($Gr < 0$). In figure 11 a set of profiles, obtained for Grashof numbers in the range $-300 \leqslant Gr \leqslant 300$ is collated, whereas all profiles are taken for a Reynolds number $Re = 39.4$ and at a distance $Z_3 = 17.75$ downstream of the body. Dimensionless profiles of the velocity components $\tilde{U}(X, Z_3)$ and $W(X, Z_3)$ are plotted in figure 11(*a*, *b*) and the sign-sensitive quantity $Gr\Theta(X, Z_3)$ is given in figure 11(*c*). The quantity $Gr\Theta$ is obtained via

$$Gr\,\Theta(X, Z) = \frac{\alpha g d^3 (T - T_\infty)}{\nu^2} \tag{4.19}$$

directly proportional to the actual temperature $[T(X, Z) - T_\infty]$ of the fluid.

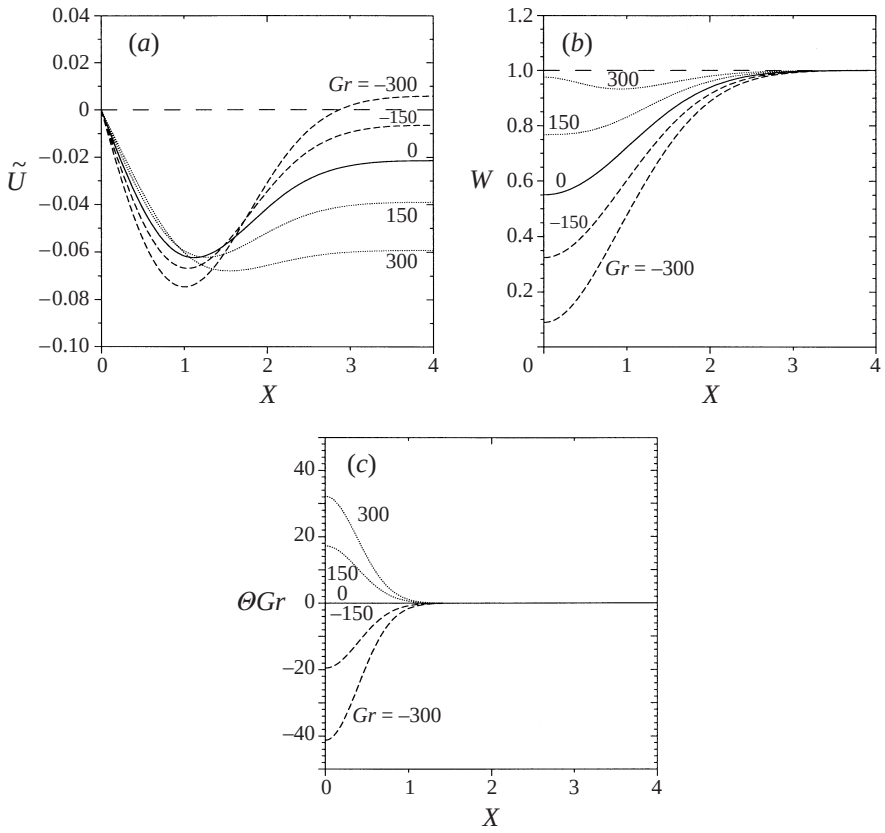

FIGURE 11. Profiles of (*a*) the dimensionless horizontal velocity $\tilde{U}(X, Z_3)$, (*b*) the dimensionless vertical velocity $W(X, Z_3)$, (*c*) the dimensionless temperature $Gr\,\Theta(X, Z_3)$ downstream of a weakly heated/weakly cooled body. The distance above the body is $Z_3 = 17.75$, the parameters are $Re = 39.4$ and $Pr = 6.13$. The other parameters are approximately $\Omega \simeq 3.5, \bar{c}_w \simeq 1.8 - 0.003Gr$.

From the temperature profiles in figure 11(*c*) we see the expected Gaussian profiles across the wake, and we find from the dotted profiles increasingly hot fluid in the wake centre for increasing Grashof numbers (cf. $Gr = 150, 300$). For $Gr = 0$ we recover the isothermal wake (solid profile). With decreasing Grashof numbers (cf. $Gr = -150, -300$) the body is cooler than the ambient fluid and, thus, the dashed temperature profiles show cold fluid in the wake centre. Independent of the Grashof number, the heated/cooled zone is of thickness $\delta_{th} \simeq 1$. The centre amplitude $Gr\,\Theta(0, Z_3)$ is found to behave like

$$Gr\,\Theta(0, Z_3) \propto Gr^{0.967}, \tag{4.20}$$

which indicates that $\Theta(X, Z)$, following equation (2.81*p*), does not develop a dependence on Gr. The form function $H(\eta)$ in equation (2.81*p*) remains independent of Gr.

The kinematic effect of the hot/cold fluid in the wake on the vertical velocity $W(X, Z_3)$ can be inspected in figure 11(*b*). Here we find an acceleration of the hot fluid in the wake centre from the dotted profiles (cf. $Gr = 150, 300$) compared to the isothermal wake ($Gr = 0$). This effect has already been discussed in §§ 4.2 and 4.3. In contrast, cold fluid in the wake is retarded due to its higher specific weight.

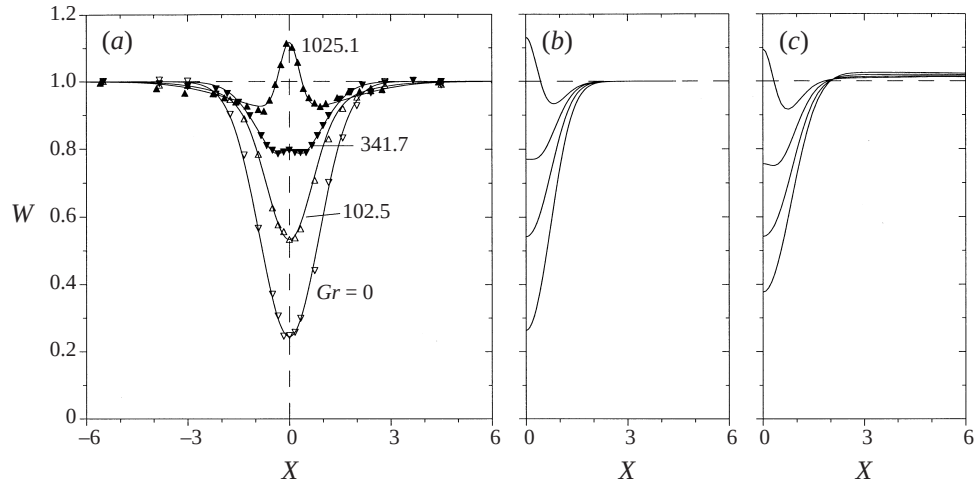

FIGURE 12. Profiles of the dimensionless vertical velocity $W(X, Z_1)$ downstream of the cylinder for various temperatures T_b: (*a*) the experimental data and corresponding least-square fits, (*b*) results from the asymptotic theory and (*c*) results from the numerical simulations. The distance above the cylinder is $Z_1 = 7.75$, the parameters are $Re = 39.4, Pr = 6.13, Gr = 0, 102.5, 341.7, 1025.1$.

This can be inferred from the dashed profiles obtained for the cooled body (cf. $Gr = -150, -300$), which show an increasingly strong velocity deficit in the wake centre. Thus, cold fluid has a similar effect to an increase of the drag coefficient, as both lead to more pronounced wake profiles. The centre amplitude $W(0, Z_3)$ of the vertical velocity almost exactly follows the proportionality

$$W(0, Z_3) \propto Gr^{1.0}. \tag{4.21}$$

As both form functions $F(\eta), K(\eta)$ in equation (2.80*p*) are independent of Gr, this is consistent with equation (2.80*p*).

The profiles of the horizontal velocity component $\tilde{U}(X, Z_3)$ are given in figure 11(*a*). For the isothermal body (cf. $Gr = 0$) the solid profile indicates a flow of ambient fluid into the wake centre ($\tilde{U} < 0$), which persists for $X \to \infty$. The heated body (cf. $Gr = 150, 300$) clearly intensifies the inward flow, as the dotted profiles show larger amplitudes for $X \to \infty$. This is a consequence of the vertical acceleration of the hot fluid in the wake centre, which in turn demands a greater supply of fluid from the ambient. If the body is cooled (cf. $Gr = -150, -300$) the situation develops quite differently. Now, the vertical retardation of the cold fluid in the wake centre may even lead to a horizontal flow outward into the ambient ($U > 0$), as can be inferred from the dashed profiles. The amplitude $\tilde{U}(X \to \infty, Z_3)$ of the horizontal velocity far outside follows the law

$$\tilde{U}(X \to \infty, Z_3) \propto Gr^{1.04}. \tag{4.22}$$

The last term in equation (2.79*p*) is responsible for the behaviour $\eta \to \infty$. Neither form functions $G(\eta), I(\eta)$ have a dependence on Gr and in all cases (2.79–2.81*p*) the dependences on Gr are explicitly given.

The influence of the Grashof number Gr on the flow field can be verified by the experimental measurements and by the numerical simulations of the vertical velocity profiles $W(X, Z_i)$. A comparison of these profiles in the plane $Z_1 = 7.75$ is given in figure 12. We see a reasonably good agreement of the profiles obtained by all three methods. The agreement holds for all Grashof numbers, whereas slight discrepancies

occur for the case of the strongly heated cylinder with $Gr = 1025.1$. Here we stress that the asymptotic model is outside its range of validity. A quantitative experimental verification can be obtained from a comparison of the measured centre amplitudes $W(0, Z_3)$ in the plane $Z_3 = 17.75$ and the power law (4.21), found from the asymptotic model. We exclude the data for $Gr = 1025.1$ and find from the experimental data the least-square fit

$$W(0, Z_3) \simeq 0.581 + 1.126 \times 10^{-2} Gr^{1.0}. \tag{4.23}$$

Thus, the experimental data to excellent accuracy confirm the linear law in the range of moderate Grashof numbers.

As shown in figures 8, 10 and 12, sufficiently large Grashof numbers lead to centreline velocities $W(0, Z) > 1$. Examining equation (2.80p) with $F(0), K(0)$ from the integrated system (2.69–2.78p), we find for fixed $Pr = 6.13$

$$\Omega Gr \geqslant 0.35 \frac{\bar{c}_w Re^3}{Z} \left(1 + 0.07 \frac{\bar{c}_w \sqrt{Re}}{\sqrt{Z}} \right). \tag{4.24}$$

Condition (4.24), consistent with all theoretical and experimental results, defines the parameter range for which the centreline velocity exceeds the free-stream velocity.

5. Conclusion

We have studied the flow and temperature fields in wakes above heated bodies. The problem is either plane for horizontal cylindrical bodies or axisymmetric for spherical bodies. We consider the laminar flow of a Newtonian fluid, subject to inertial forces, viscous forces and buoyant forces. Buoyant forces are modelled by using the Boussinesq approximation. This mixed-convection problem is characterized by three dimensionless groups, namely the Reynolds number, the Grashof number and the Prandtl number.

We use three principle means of investigation. (*a*) An asymptotic model is developed, which, based on boundary-layer theory, is valid for large Reynolds numbers and large Péclet numbers. Further expansions focus on the far wake and on weak buoyant forces. The model provides analytical expressions in self-similar form for the flow and temperature fields, containing explicit parameter dependences, in conjunction with a system of ordinary differential equations for the shape functions. To validate the asymptotic model, experiments and FEM simulations in a plane geometry are employed. (*b*) The experiments are performed in a vertical water channel ($Pr \simeq 6$), where a horizontal isothermal cylinder is positioned. Profiles of vertical velocity and temperature are measured at distances $7.75 \leqslant z/d \leqslant 17.75$ above the cylinder by means of laser Doppler anemometry and thermocouples. The parameter range in the experiments is $Re \simeq 40$, $0 \leqslant Gr \leqslant 1025$. (*c*) The FEM simulations use a commercial code (FIDAP 7.6) to compute the flow and temperature fields on a mesh of about 25 000 nodes. The computational domain extends sufficiently outward horizontally from the symmetry line, i.e. $0 \leqslant x/d \leqslant 30$. Vertically it extends sufficiently far into both upstream and downstream direction and covers the range $-50 \leqslant z/d \leqslant 60$.

In the heated wake above the cylinder we find buoyant forces, governed by the group Gr/Re^2, leading to an acceleration of the fluid, which tends to reduce the velocity deficit in the wake centre. For strong heating this acceleration may even lead to vertical velocity amplitudes larger than the forced flow amplitude. The amplitude of the buoyant contribution to the vertical velocity profile increases with increasing Grashof number. In conjunction with the vertical movement of fluid, horizontal transport of

fluid from far outside into the wake centre is characteristic for the isothermal wake. For the heated wake strong buoyant forces cause an intense horizontal transport of fluid into the wake centre. The horizontal velocity far outside the wake increases likewise with increasing Grashof number. For a cooled wake, instead, retardation of the fluid in the wake centre occurs. This reduces the horizontal flow into the wake centre and may even cause a horizontal flow outward.

The Prantdl number governs the width of the thermal wake, which in general is different from the width of the kinematic wake. Small Prandtl numbers result in a wide thermal wake causing buoyant forces across and beyond the kinematic wake. Thus, as heat is distributed over a wide area, a wide buoyant plume with weak acceleration is present. In contrast, large Prandtl numbers are responsible for narrow thermal wakes, liberating buoyant forces in a narrow subregion of the kinematic wake. Thus, a slender buoyant plume in the wake centre with strong acceleration develops.

The asymptotic model has been carefully validated against both experiments and FEM simulations for plane geometry. As the model has also been developed for axisymmetric geometry, an experimental or numerical validation of this would be worthwhile. Further, the laminar assumption is restricted to a limited parameter range. An extension of the present model to turbulent flow would also be attractive. In fact, the Reynolds-averaged conservation equations could serve as a basis for the development of an analogous turbulent model. Using similar approximations, the equations for the time-averaged velocities and temperature are almost identical with the laminar set of equations. However, a turbulent shear stress and a turbulent heat flux are present as opposed to the diffusive terms in the laminar set of equations. Here, reasonable closure conditions would be required.

I would like to thank my students F. Fellmoser, R. Griesbaum, V. Sarnes and A. Wintruff, who all contributed to this work while elaborating their diploma thesis at the University of Karlsruhe, respectively the Engineering College of Karlsruhe. Moreover, I would like to acknowledge the contribution of my student U. Siegel from the Engineering College of Offenburg, who was involved in the comparing computations and plots during the preparation of this manuscript.

This article is dedicated to Professor Dr.-Ing. U. Müller on the occasion of his (semi) retirement. He has been an inspiring teacher to me all these years.

REFERENCES

Afzal, N. 1981 Mixed convection in a two-dimensional buoyant plume. *J. Fluid Mech.* **105**, 347–368.

Afzal, N. 1983 Mixed convection in an axisymmetric buoyant plume. *Intl J. Heat Mass Transfer* **26**, 381–388.

Afzal, N. 1985 Mixed convection plume above a point heat source in a vertical free stream. *Intl J. Heat Mass Transfer* **28**, 2043–2047.

Berger, S. A. 1968 The incompressible laminar axisymmetric far wake. *J. Maths Phys.* **47**, 292–309.

Berger, S. A. 1971 *Laminar Wakes.* Elsevier.

Betchov, R. & Criminale, W. O. 1967 *Stability of Parallel Flows.* Academic.

Brand, R. S. & Lahey, F. J. 1967 Heated laminar vertical jet. *J. Fluid Mech.* **29**, 305–315.

Brodowicz, K. & Kierkus, W. T. 1966 Experimental investigation of laminar free convection flow in air above horizontal wire with constant heat flux. *Intl J. Heat Mass Transfer* **9**, 81–94.

Churchill, S. W. & Chu, H. H. S. 1975 Correlating equations for laminar and turbulent free convection from a horizontal cylinder. *Intl J. Heat Mass Transfer* **18**, 1049–1053.

Collis, D. C. & Williams, M. J. 1959 Two-dimensional convection from heated wire at low Reynolds numbers. *J. Fluid Mech.* **6**, 357–384.

Crane, L. J. 1975 Axially symmetric plumes at very small Prandtl numbers. *J. Appl. Maths Phys.* **26**, 427–435.

Forstrom, R. J. & Sparrow, E. M. 1967 Experiments on the buoyant plume above a heated horizontal wire. *Intl J. Heat Mass Transfer* **10**, 321–331.

Fujii, T. 1963 Theory of the steady laminar natural convection above a horizontal line heat source and a point heat source. *Intl J. Heat Mass Transfer* **6**, 597–606.

Fujii, T., Morioka, I. & Uehara, H. 1973 Buoyant plume above a horizontal line heat source. *Intl J. Heat Mass Transfer* **16**, 755–768.

Gebhart, B., Jaluria, Y., Mahajan, R. L., Sammakia, B. 1988 *Buoyancy-Induced Flow and Transport*. Hemisphere.

Gebhart, B. & Pera, L. 1970 Mixed convection from long horizontal cylinders. *J. Fluid Mech.* **45**, 49–64.

Gebhart, B., Pera, L. & Schorr, A. W. 1970 Steady laminar natural convection plumes above a horizontal line source. *Intl J. Heat Mass Transfer* **13**, 161–171.

Gnielinski, V. 1975 Berechnung mittlerer Wärme- und Stoffübergangskoeffizienten an laminar und turbulent überströmten Einzelkörpern mit Hilfe einer einheitlichen Gleichung. *Forsch.-Ing. Wesen* **41** (5), 145–153.

Goldstein, S. 1933 On the two-dimensional steady flow of a viscous fluid behind a solid body. *Proc. R. Soc. Lond.* A **142**, 545–562.

Hatton, A. P., James, D. D. & Swire, H. W. 1970 Combined forced and natural convection with low-speed air flow over horizontal cylinders. *J. Fluid Mech.* **42**, 17–31.

Hieber, C. A. & Gebhart, B. 1969 Mixed convection from a sphere at small Reynolds and Grashof numbers. *J. Fluid Mech.* **38**, 137–159.

Kuiken, H. K. & Rotem, Z. 1971 Asymptotic solution for plume at very large and small Prandtl numbers. *J. Fluid Mech.* **45**, 585–600.

Liñán, A. & Kurdyumov, V. N. 1998 Laminar free convection induced by a line heat source, and heat transfer from wires at small Grashof numbers. *J. Fluid Mech.* **362**, 199–227.

Loitsianski, L. G. 1967 *Laminare Grenzschichten*. Akademie, Berlin.

Lugt, H. J. 1979 *Wirbelströmung in Natur und Technik*. G. Braun, Karlsruhe.

Riley, D. S. & Drake, D. G. 1983 Mixed convection in an axisymmetric buoyant plume. *Q. J. Mech. Appl. Maths* **36**, 43–54.

Rouse, H., Yih, C. S. & Humphreys, H. W. 1952 Gravitational convection from a boundary source. *Tellus* **4**, 201–210.

Schlichting, H. 1982 *Grenzschicht-Theorie*. Braun, Karlsruhe.

Schuh, H. 1948 Boundary layers of temperature. In *Boundary Layers* (ed. W. Tollmien). British Ministry of Supply, German Document Centre, Reference 3220T.

Spalding, D. B. & Cruddace, R. G. 1961 Theory of the steady laminar buoyant flow above a line heat source in a fluid of large Prandtl number and temperature-dependent viscosity. *Intl J. Heat Mass Transfer* **3**, 55–59.

Stewartson, K. 1957 On asymptotic expansions in the theory of boundary layers. *J. Math. Phys.* **36**, 173–191.

Tollmien, W. 1931 Grenzschichtheorie. In *Handbuch der Experimentalphysik*, Bd. IV, pp. 242–287. Akademie, Leipzig.

Weast, R. C. 1980 *Handbook of Chemistry and Physics*, 61st edn. CRC Press.

Wesseling, P. 1975 An asymptotic solution for slightly buoyant laminar plumes. *J. Fluid Mech.* **70**, 81–87.

Wood, W. W. 1972 Free and forced convection from fine hot wires. *J. Fluid Mech.* **55**, 419–438.

Yih, C.-S. 1951 Free convection due to a point source of heat. *Proc. 1st US Natl Congr. Appl. Mech.*, pp. 941–947.

Yih, C.-S. 1952 Laminar free convection due to a line source of heat. *Trans. Am. Geophys. Union* **33**, 669–672.

Zeldovich, Ya.B. 1937 The asymptotic laws of freely-ascending convective flows. *Zh. Eksp. Teor. Fiz.* **7**, 1463–1465.

Žukauska, A. & Žiugžda, J. 1985 Heat transfer of a cylinder in crossflow. In *Experimental and Applied Heat Transfer Guide Books* (ed. G. F. Hewitt). Hemisphere.